Ann. nucl. Energy, Vol. 9, pp. 443 to 472, 1982
Printed in Great Britain

0306-4549/82/090443-30 $03.00/0
Pergamon Press Ltd

INVESTIGATION OF SPACE–ENERGY EFFECTS IN THE REACTIVITY MEASUREMENT BY NEUTRON NOISE WITH EXCORE DETECTORS IN A REFLECTED LWR

V. H. LESCANO* and K. BEHRINGER
Swiss Federal Institute for Reactor Research (EIR), CH-5303 Würenlingen, Switzerland

(*Received* 10 *August* 1981; *accepted in revised form* 29 *April* 1982)

Abstract—Practical application of the zero-crossing correlation method for measuring slightly-subcritical reactivities in a swimming-pool reactor required the use of detector locations in the reflector zone near to the core boundary. Experimental investigations of neutron-noise cross-power spectra showed significant deviations from the point-reactor model at higher frequencies (> 100 Hz). Nevertheless, the use of the point-reactor model was found to be a useful approach in the analysis of the zero-crossing correlation method, yielding results which agreed well with those obtained from the rod-drop method. The theoretical part of the work is concerned with a space-dependent model calculation in two-group diffusion theory to support the experimental findings. The model calculation can explain the trends observed in the neutron-noise spectra as well as the applicability of the point-reactor model to the zero-crossing correlation method. To obtain better insight, the calculations have been extended to neutron-noise spectra when one or both detectors are located in the core zone. In the case of a large core and widely-spaced detectors, with at least one detector in the core zone, a sink frequency appears in the spectra. This effect is well known in coupled-core kinetics.

1. INTRODUCTION

The application of neutron-noise analysis to measure or monitor slightly-subcritical reactor states is a well-known technique (see Seifritz and Stegemann, 1971; Saito, 1979, for reviews). A special on-line correlation method in the time domain, established as the 'Zero-Crossing Correlation Method', has been developed at EIR (Behringer *et al.*, 1974a,b, 1975). It is based on a two-detector measuring device and special signal conditioning to extract the prompt-neutron kinetics information. The method was originally developed for a reactor system with slow prompt-neutron kinetics. It was used in practice on the DO_2-moderated reactor DIORIT which has been out of operation for several years. Successful investigation of the method was also performed on the graphite-moderated critical facility KAHTER (Süssmann *et al.*, 1976). The method is general and can also advantageously be applied to faster kinetic systems. Plans are currently being made to use this reactivity meter on the swimming-pool reactor SAPHIR as an item of operating equipment. The core of the reactor SAPHIR does not allow a proper incore instrumentation as normally used for this type of neutron-noise analysis application, since the neutron detectors can normally be located only in the reflector zone near the core boundary.

The determination of subcritical reactivities by means of the prompt-neutron kinetics requires a frequency range for the analysis which must exceed the break frequency of the reactivity transfer function. But, even for small-reactor systems, the appearance of higher modes cannot be disregarded at higher frequencies and may introduce spatial effects. Therefore, the use of the point-reactor model to analyse the experimental data can introduce sources of systematical error in the evaluation.

In the original application of the reactivity meter at the reactor DIORIT, there was no need to search for spatial effects. Both detectors were well centred in the core. Experiments performed by Buhl *et al.* (1968) in a large zero-power natural uranium graphite-moderated reactor indicated that simple point-reactor kinetics adequately describe the neutron-noise spectra everywhere except near to the core edges. On the other hand, the roll-off of neutron cross-power spectra measured by Thomas *et al.* (1973) on a large D_2O-facility does not seem to be in agreement with the point-kinetics prediction, even for the case of central detector locations.

There is an intuitive feeling that measurements to be performed especially in the reflector (at the position of the thermal flux peak) should be influenced by both space and energy effects. Measurements of cross-power spectra, which were begun on the reactor SAPHIR, showed the appearance of significant deviations from the point-kinetics behaviour at higher frequencies

*IAEA/EIR fellow. Permanent address: Comisión Nacional de Energía Atómica (CNEA), Buenos Aires, Argentina.

(> 100 Hz). This finding is somewhat contrary to the results obtained by Ricker *et al.* (1968) on a light-water pool-type facility who concluded that the point-kinetics model is valid up to 1 kHz. Since only auto-power spectra were measured, the detection-noise component was a parameter determined by the data fit. The analysis, therefore, may not be sufficiently sensitive to reveal high-frequency effects.

The main aim of this work is to give theoretical support to the experimental findings and to investigate on a simple 1-D reflected-reactor model in two-group diffusion theory how far space–energy effects will be involved. In the numerical results typical data for a highly-enriched reflected LWR are used. Our treatment follows basically the space-dependent neutron-noise theory developed by Sheff and Albrecht (1966a,b) in one energy group. The calculation procedure is extended to two energy groups and applied to the reflected-reactor model.

In Section 2, the concept of the model is explained, and the associated problems and assumptions to be made are compiled. The quantity, which is to be calculated and investigated as a function of the system reactivity, the nuclear parameters, the core size and the detector locations, is the cross-power spectral density of the count-rate fluctuations between the two detectors. The application of the inverse Fourier transform to this quantity, imposed with the filter function of the signal conditioner, gives the corresponding cross-correlation function and the dependence of its zero-crossing point on the reactivity. Section 3 is concerned with the general problem of how system fluctuating quantities will spatially affect the count-rate cross-power spectral density. The treatment is based on first-order kinetic perturbation theory using Langevin techniques. The derived relation is then applied to the input neutron processes by introducing noise-equivalent sources specifically responsible for the appearance of correlations between the detector signals. Since the major interest is in the shapes of the spectra, possibilities of comparing them with a reference spectrum yielding space-independent results are considered in Section 4. Section 5 describes the experimental investigations and summarizes their results before proceeding to the numerical results of the model calculation which are discussed in Section 6. In order to get better insight into the space effects, the calculations also include cases of neutron spectra when one or both detectors are located in the core zone. In Section 7 the conclusions are summarized.

2. MODEL ASSUMPTIONS AND ASSOCIATED PROBLEMS

The model is shown in Fig. 1. It represents a 1-D reactor system consisting of a homogeneous core, which gives good thermalization of the neutrons, and an infinite homogeneous reflector on the right-hand side. The moderating material in the core and the reflector material is water.

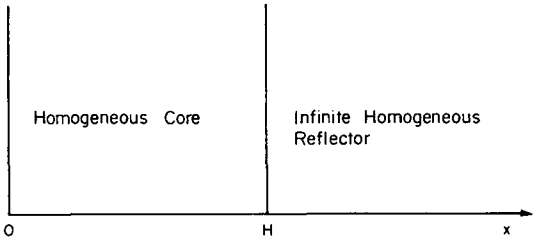

Fig. 1. Reflected reactor model.

It should be emphasized that numerical results derived from simple-model assumptions are certainly not sufficient to be applied to the actual reactor conditions. SAPHIR is a research reactor (5 MW(th)). Its core configuration does not have simple rectangular geometry, and is changed when a fuel element shuffling is made. On one side, a Be-reflector bank is normally used. The strongly asymmetrical and inhomogeneous core does not facilitate the comparison of experimental data with the results of simple theoretical calculations. Nevertheless, the chosen reflected assembly is the simplest model that can be handled analytically with relative ease, and is believed to give meaningful results. The theoretical treatment will be based on the two-group diffusion equations which are the minimum requirement for handling this type of problem. Whereas for the static flux calculations there is no important difference in the formalism when one would consider a symmetrical reflected system, the latter would make the space-dependent treatment of the neutron noise into a three-regional problem. An additional reflector on the left-hand side is expected to have little influence on the points of observation in the reflector zone of the right-hand side. It would unnecessarily complicate the mathematics and require the use of a computer at a much earlier stage.

The detectors are supposed to be of the 'point' type. This means, in a 1-D treatment, that physically they have the shape of a very thin plate in parallel to the slab geometry of the reactor system. With regard to the purpose of our investigations the numerical calculations are based on the assumption that both detectors are only sensitive to thermal neutrons and have identical detection characteristics. The general theory, however, includes the option that a detector might also, or exclusively, be sensitive to fast neutrons. There is an interesting note by Penland *et al.* (1971) who measured neutron lifetimes in the core and in the reflector of a

pool critical assembly by means of a thermal–fast neutron detector combination. Specifically, the fast-thermal CPSD-technique allows measurement of the thermal-neutron lifetime independent of the delayed-neutron fraction. This possibility was predicted by Nieto *et al.* (1968) using a two-energy group space-independent model, and by Ackermann *et al.* (1971) who extended the model to a reflected system in two energy groups and two space nodes. A two-detector measuring device eliminates the detection-noise component which is uncorrelated between both detector signals and would otherwise be a dominant background. Since every neutron detector operated as an ionization chamber in the current mode has a certain inevitable sensitivity to γ-radiation, the application of this technique becomes imperative in subcriticality measurements on power reactors for the γ-rejection (Penland and Hanauer, 1968).

We follow the practice, adopted in most neutron-noise theories, of neglecting the depression of the surrounding flux due to the presence of a detector. The effect of a detector perturbation may influence the interpretation of noise-spectra in water-moderated systems (Williams, 1974). The detector tends to sample preferentially from shorter chains, simply because there are relatively more of these in its neighbourhood. We feel that such an effect should be less pronounced for excore detectors. In our model, we assume a fast stationary neutron source in the core with a distribution corresponding to the critical thermal flux. With this assumption higher static modes do not exist in the unperturbed subcritical system. Throughout this paper the static reactivity concept associated with the fundamental eigenvalue of the static reactor equations is used (Gozani, 1963).

A first estimate of the zero-power kinetic behaviour of reflected reactors has been given by Cohn (1962). A simple two-point model (core and reflector) was used. Within each region the theory is space-independent and assumes one energy group. It was found that with typical data for a thermal reactor the source transfer function in the core has the same shape as the equivalent bare-reactor transfer function in the frequency range up to the break frequency. Some deviations appear at higher frequencies. The same approach was used by Randall and Griffin (1964) to derive an expression for the power spectral density of the noise in the reflector. Cohn (1964) later extended his model to two energy groups. It seems to us that if, in this type of model (see also Ackermann *et al.*, 1971), one simply keeps adding regions and coupling coefficients, then there is a tendency to oversimplify the kinetic behaviour of the system by considering spatially-independent regions.

A useful space-dependent neutron-noise theory using one-group diffusion equations has been developed by Sheff and Albrecht (1966a,b). First-order kinetic perturbation theory and Langevin techniques are applied to obtain an output correlation function in terms of an input-noise correlation function as a double convolution over two system Green's function. Noise-equivalent source terms present within the system are introduced by means of the Schottky formula. The theory has especially been applied to the case of a bare unreflected cubic reactor to demonstrate that, even when the extraneous source distribution is assumed to be fundamental mode, distinct spatial effects can be expected in the detector noise spectra. Our treatment of the reflected-reactor model in two energy groups basically follows these ideas. Adjoint function techniques in the frequency domain are used. Sheff (1969) states that, in the calculation of space–energy-dependent detector noise spectra, a two-group approximation is not representative of experiments that are possible in thermal reactors. He suggests that a treatment in at least three energy groups is required. We agree insofar as, in LWRs, the neutron spectrum is relatively hard. A multigroup treatment of the noise may certainly give quantitatively improved results. On the other hand, the two-group diffusion equations contain all the information that is essential for describing energy effects. In the solution of the kinetic eigenvalue problem of a bare homogeneous reactor there are two roots, a μ-root and a λ-root. The Green's function in the frequency domain is correspondingly composed of a μ-component and a λ-component in each energy group. Each component is a solution of the kinetic equations which has to satisfy the condition of vanishing at the core boundaries. The μ-component has a spatial range of the order of the reactor size and contains (though not exclusively) the reactivity transfer function (for more details see Behringer *et al.*, 1979a; and Appendix C). The λ-component represents a neutron-spectrum effect which is reflected in space with a short relaxation length of the order of the thermal diffusion length. Its contribution to the detector response is completely negligible at lower frequencies as long as reactivity-induced fluctuations are dominant in the spectra. Analytis (1982) has recently investigated this μ- and λ-component concept of the neutron noise in three energy groups. He showed that the detector response to the neutron-noise field in homogeneous media can be separated into a component with a long relaxation length (μ-component) and two spatially-localized components (λ_1, λ_2-components), whose relaxation lengths in water-moderated reactors are similar and of the order of the thermal diffusion length. This result implies that in an M multigroup treatment

of the noise in water-moderated reactors there is one long range μ-component and $M-1$ very local λ-components which all have relaxation lengths of the same order of magnitude and may represent only a fine splitting of the two-group λ-component. In the two-group treatment of the noise in a reflected system, the μ-component and the λ-component are not distinct and separate solutions of the Green's function equations. They are coupled via the interface boundary conditions. As shown by Pázsit (1978), in particular an appreciable contribution of the λ-component to the detector response at the position of the thermal flux peak in the reflector can be expected.

3. COUNT-RATE CROSS-POWER SPECTRAL DENSITY DUE TO THE FISSION BRANCHING PROCESS

The time-dependent two-group diffusion equations are given by

$$\text{div } D_1 \text{ grad } \phi_1 - \Sigma_1\phi_1 + \nu\Sigma_f(1-\beta)\phi_2 + \sum_i \lambda_i C_i + Q = \frac{1}{v_1}\frac{\partial\phi_1}{\partial t} \quad (1a)$$

$$\text{div } D_2 \text{ grad } \phi_2 - \Sigma_2\phi_2 + \Sigma_R\phi_1 = \frac{1}{v_2}\frac{\partial\phi_2}{\partial t} \quad (1b)$$

$$\frac{\partial C_i}{\partial t} = -\lambda_i C_i + \beta_i \nu\Sigma_f\phi_2, \quad (1c)$$

where all symbols have their usual meaning

ϕ_1, ϕ_2 = fast and thermal neutron flux response
D_1, D_2 = diffusion coefficients
$\Sigma_1 = \Sigma_{a1} + \Sigma_R$
$\Sigma_2 = \Sigma_{a2}$
Σ_{a1}, Σ_{a2} = absorption cross sections
Σ_R = removal cross section
$\nu\Sigma_f$ = thermal fission cross section multiplied by the average number of neutrons emitted per fission
Q = density of an extraneous fast neutron source (assumed to be distributed within the reactor system)
C_i = precursor density of the delayed neutron group i
λ_i = decay constant of C_i
β_i = effective fraction of delayed neutrons of group i
$\beta = \sum_i \beta_i$
v_1, v_2 = neutron velocity in the fast and thermal group.

Fast fission has been neglected. The group parameters and the extraneous source term are considered to be generally space- and time-dependent. According to the two-group approach concept, the fast- and thermal-neutron velocities are regarded as constants throughout the reactor system. Neutrons can only jump from v_1 to v_2. The β_i's are also treated as constants. A β_i can be considered as the conditional probability that given a neutron is emitted, it will be a delayed neutron from group i (Sheff and Albrecht, 1966a). The two-group diffusion equations must be solved with the boundary condition that the fluxes have to vanish at the (extrapolated) system surface.

Let us consider the case in which the reactor is at first in a stationary subcritical state in equilibrium with a time-constant extraneous source. The static fluxes are given in matrix notation by

$$m_{op}\begin{pmatrix}\phi_1\\ \phi_2\end{pmatrix} + \begin{pmatrix}Q\\ 0\end{pmatrix} = 0 \quad (2a)$$

with

$$m_{op} = \begin{pmatrix}\text{div } D_1 \text{ grad} - \Sigma_1, & \nu\Sigma_f\\ \Sigma_R, & \text{div } D_2 \text{ grad} - \Sigma_2\end{pmatrix}, \quad (2b)$$

where the group parameters are functions of the space-vector $\mathbf{x}$ only. We perturb the stationary reactor system by small stochastic fluctuations of the group parameters and the extraneous source. We assume ergodicity of the random processes. These fluctuations (with zero expectation values) produce fluctuations of the neutron fluxes and the precursor densities. We locate a neutron detector of very small size (point detector) at $\mathbf{x}_1$ within the reactor system. Its average count-rate per unit detector volume is

$$R(\mathbf{x}_1) = \Sigma_{1d}\phi_1(\mathbf{x}_1) + \Sigma_{2d}\phi_2(\mathbf{x}_2), \quad (3)$$

where Σ_{1d}, Σ_{2d} = detection cross section of fast and thermal neutrons, respectively.

If the fluxes are fluctuating, the count-rate* will also fluctuate. Its fluctuating part is given in the frequency domain by

$$\delta R(\mathbf{x}_1, \omega) = \Sigma_{1d}\delta\phi_1(\mathbf{x}_1, \omega) + \Sigma_{2d}\delta\phi_2(\mathbf{x}, \omega). \quad (4)$$

The count-rate spectrum can be related to the fluctuating parts of the group parameters and the extraneous neutron source by using adjoint-function techniques (van Dam, 1976; Behringer *et al.*, 1977, 1979).

$$\delta R(\mathbf{x}_1, \omega) = \int dV(\phi_1^+, \phi_2^+)\left[P_{op}\begin{pmatrix}\phi_1\\ \phi_2\end{pmatrix} + \begin{pmatrix}\delta Q\\ 0\end{pmatrix}\right] \quad (5)$$

* In what follows we use the count-rate per unit volume except where explicitly stated to the contrary.

Equation (5) represents the linear detector response to spatially-distributed perturbations. The parametric perturbation operator P_{op} is given by

$$P_{op} = \begin{pmatrix} \text{div } \delta D_1 \text{ grad} - \delta\Sigma_1, & \delta(\nu\Sigma_f)(1-h) \\ \delta\Sigma_R, & \text{div } \delta D_2 \text{ grad} - \delta\Sigma_2 \end{pmatrix} \quad (6)$$

where

$$h = j\omega \sum_i \frac{\beta_i}{\lambda_i + j\omega} \quad (7)$$

ω = angular frequency.

All fluctuating terms are functions of the space-vector $\mathbf{x}$ and the frequency ω. ϕ_1^+, ϕ_2^+ are adjoint functions which we will call the kinetic importance functions. They are defined by

$$M_{op}^+ \begin{pmatrix} \phi_1^+ \\ \phi_2^+ \end{pmatrix} = -\delta(\mathbf{x}-\mathbf{x}_1) \begin{pmatrix} \Sigma_{1d} \\ \Sigma_{2d} \end{pmatrix} \quad (8a)$$

with the adjoint operator

$$M_{op}^+ = \begin{pmatrix} \text{div } D_1 \text{ grad} - \Sigma_1', & \Sigma_R \\ \nu\Sigma_f(1-h), & \text{div } D_2 \text{ grad} - \Sigma_2' \end{pmatrix} \quad (8b)$$

where

$$\Sigma_1' = \Sigma_1 + \frac{j\omega}{v_1} \quad (8c)$$

$$\Sigma_2' = \Sigma_2 + \frac{j\omega}{v_2} \quad (8d)$$

$\delta(\mathbf{x}-\mathbf{x}_1)$ denotes the Dirac delta function. ϕ_1^+, ϕ_2^+ are functions of $\mathbf{x}, \mathbf{x}_1$ and ω. They are space-adjoint Green's functions in the frequency domain. They can also be regarded as transfer functions between a perturbation occurring at point $\mathbf{x}$ and the detector response at the point of observation $\mathbf{x}_1$. The reactor perturbations are a space-continuous multiple input and the detector acts as a single output system.

The representation of equation (5) in the frequency domain has the advantage of being more convenient and transparent than the representation formulated in the time domain, where a time-convolution integral additionally appears. The whole formalism can easily be extended to multigroup treatment. A general version in transport theory has been elaborated by van Dam (1977). By applying equation (5) to a second point detector located at $\mathbf{x}_2$ within the system (where this second detector is presumed to have the same detection characteristics as the first one), the one-sided count-rate cross-power spectral density CPSD_R (per square unit of detector volume) follows from (e.g. Bendat and Piersol, 1971)

$$\text{CPSD}_R(\mathbf{x}_1,\mathbf{x}_2,\omega) = 2 \lim_{T\to\infty} \frac{\langle \delta R^*(\mathbf{x}_1,\omega,T)\delta R(\mathbf{x}_2,\omega,T)\rangle}{T}, \quad (9)$$

considering that truncated records of finite time-length T have implicitly been used for establishing equation (5). The angle brackets in equation (9) denote the ensemble average is taken. In the same way ensemble averages must be taken between pairs of the various input signals. When one writes

$$\begin{pmatrix} \delta S_1 \\ \delta S_2 \end{pmatrix} = P_{op} \begin{pmatrix} \phi_1 \\ \phi_2 \end{pmatrix} + \begin{pmatrix} \delta Q \\ 0 \end{pmatrix} \quad (10)$$

the output CPSD_R can be expressed by the input CPSDs related to the fluctuations δS_1, δS_2.

$$\text{CPSD}_R(\mathbf{x}_1,\mathbf{x}_2,\omega) = \sum_{\substack{i,k \\ (i,k=1,2)}} \int\int \mathrm{d}V\, \mathrm{d}V' \phi_i^{+*}(\mathbf{x},\mathbf{x}_1,\omega) \times \text{CPSD}_{S_{ik}}(\mathbf{x},\mathbf{x}',\omega)\phi_k^+(\mathbf{x}',\mathbf{x}_2,\omega), \quad (11)$$

i, k refer to group indices.

Due to equation (10) each $\text{CPSD}_{S_{ik}}$ is composed of a subset of input CPSDs from the various individual processes and possible cross-terms in general. Equation (11) indicates, how their contributions to the output CPSD_R are to be weighted by the kinetic importance functions. Equation (11) gives a general basis for treating the space phenomena appearing in neutron noise. There is one exception: equation (11) can be used for describing the CPSD_R of a two-detector measuring device by making further assumptions concerning the noise sources. In zero-power reactors, though, it does not hold for computing count-rate auto-power spectral densities. The reason for this is that one has to consider not only the various input processes involved in the neutron field but also the detection process itself which cannot be isolated.

The input neutron processes as far as they contribute to the CPSD_R are sharply localized in space. There is no space-correlation except for identical space points. Hence, writing

$$\text{CPSD}_{S_{ik}}(\mathbf{x},\mathbf{x}',\omega) = S_{ik}(\mathbf{x},\omega)\delta(\mathbf{x}-\mathbf{x}') \quad (12)$$

and substituting the input CPSDs in equation (11) by equation (12) results in the output CPSD:

$$\text{CPSD}_R(\mathbf{x}_1,\mathbf{x}_2,\omega) = \sum_{i,k} \int \mathrm{d}V \phi_i^{+*}(\mathbf{x},\mathbf{x}_1,\omega) \times S_{ik}(\mathbf{x},\omega)\phi_k^+(\mathbf{x},\mathbf{x}_2,\omega). \quad (13)$$

The further assumption needed to make the Langevin method applicable, and to obtain useful results through application of equation (13), is the Schottky formula (Cohn, 1960).* This is a noise-equivalent source for the

* Saito (1967a) showed that the Schottky formula is not necessarily a specific assumption but rather the consequence of a more general assumption that the macrostochastical variables characterizing the state of a nuclear system behave as if they were Markovian.

input and is particularly suitable for representing discrete random phenomena. For a source term S_{ik} as input to equation (13), the formula reads

$$S_{ik} = 2\sum_l q_l^2 \bar{m}_l, \tag{14}$$

where q_l is the net number of neutrons produced (or removed) in the occurrence of one nuclear reaction of type l, and $\bar{m}_l$ is the average reaction rate of type l occurring per unit volume. In equation (14) the assumption is implicitly made that the various reaction processes are independent.

The Schottky formula is the result of a white-noise assumption. The approximation is valid up to frequencies of the order of the reciprocal of the mean reaction time of a process. The kinetic importance functions, however, act as low-pass filters cutting the high-frequency input components in a frequency region which is much lower than the validity range of the Schottky formula.

Saito (1967a) has extensively studied the properties of the random noise sources which give rise to the inherent statistical fluctuations in nuclear reactors. We have to distinguish between single- and paired-neutron contributions. In general, for example, absorption, scattering and emission from the extraneous source are single-neutron effects. The fission term, however, results in both single- and paired-neutron contributions. Other paired-neutron effects, which will not be included here, can arise from multiple emission by a radioactive decay in an extraneous source or from the (n, 2n) reaction in a Be-reflector.

A detector removes a neutron when it detects it. The detection process destroys any single-neutron correlation which, otherwise, the neutron would have in the future. Single-neutron effects contribute either nothing (e.g. leaking neutrons) or only to the variance of the count-rate, i.e. they appear only in the so-called detection-noise component which is a (dominant) white-noise term in the one-detector count-rate APSD. As used up to this point, equation (13) gives an incomplete description of a count-rate APSD. It represents in this case only the paired-neutron contribution. The detection-noise component is uncorrelated between two detectors and is eliminated by a two-detector cross-correlation measuring device. The only term which remains as a contribution to the CPSD_R is the paired-neutron effect in the fission process. The fission process appears in the signal δS_1 of equation (10) as

$$\delta S_1 = (1-h)\Sigma_f \phi_2 \delta\nu. \tag{15}$$

A problem which has led to some discussion (Sheff and Albrecht, 1966a; Saito, 1967b) is the applicability of the Schottky formula when delayed neutrons are included. $\delta\nu$ is the fluctuation in the total number of neutrons ($=\delta\nu_p$ prompt neutrons $+\delta\nu_d$ delayed neutrons) per fission. The processes of prompt- and delayed-neutron emission are not independent—as application of the Schottky formula would require. The mean lifetime for the ith group of delayed neutrons is $1/\lambda_i$, which is clearly of such order as to make the white-noise assumption for delayed neutrons invalid. On the other hand, one can regard a delayed neutron as a neutron 'stored' in a precursor particle which is instantaneously generated by fission. Since we have eliminated the fluctuations of the precursor densities and used a reduced number of stochastic variables, the retardation effect induced by the temporary 'storage' in precursors appears in equation (15) as a feedback to the neutron field via the frequency-dependent factor $1-h$. According to this consideration, we have therefore to apply the Schottky formula to the total number of neutrons emitted by fission. Combining equations (15) and (14) with $q_{\nu'} = \nu' - 1$ and $\bar{m}_{\nu'} = \Sigma_f \phi_2 P_{\nu'}$, where $P_{\nu'}$, is the probability of a given fission emitting totally ν' neutrons, and separating the paired-neutron effect appearing as $\nu'(\nu'-1)$ ordered pairs, result in the noise-equivalent source:

$$S_{11} = 2|1-h|^2 \overline{\nu(\nu-1)}\Sigma_f \phi_2. \tag{16}$$

Inserting equation (16) into equation (13) gives the final result for the CPSD_R due to the fission branching process initiated by thermal neutrons:

$$\mathrm{CPSD}_R(\mathbf{x}_1, \mathbf{x}_2, \omega) = 2|1-h|^2 \frac{\overline{\nu(\nu-1)}}{\nu} \times \int \mathrm{d}V \phi_1^+{}^*(\mathbf{x}, \mathbf{x}_1, \omega)\nu\Sigma_f(\mathbf{x})\phi_2(\mathbf{x})\phi_1^+(\mathbf{x}, \mathbf{x}_2, \omega). \tag{17}$$

The result is consistent with the one-energy group approach.

Theoretically, one can bring the second detector to the location of the first one. Equation (17) remains valid, because even overlapping detectors are different detectors.

For the evaluation of equation (17), the static fluxes and kinetic importance functions must be known. A standard method for solving the static and kinetic equations is to use series expansions in space-eigenfunctions and to approximate the result with a limited number of terms. In our 1-D model, however, the kinetic problem can be solved in an analytically closed form. This was first remarked by Sheff (1968). For the static subcritical fluxes we assume the shapes of the critical fluxes. The explicit expressions for the static fluxes are given in Appendix A. The solution of the kinetic importance functions are represented in

Appendix B for both an excore detector and an incore detector. Since the space-dependence in all these functions appears via trigonometric and exponential functions, the integral in equation (17) can readily be evaluated. The numerical evaluation then only requires simple programming work.

4. REFERENCE GLOBAL POWER SPECTRAL DENSITY

The major interest in the application of the zero-crossing correlation method to reactivity determination is the spectral shape of the $CPSD_R$ for any detector location chosen in the system. In order to have available a basis for comparison of how strongly the spectral shape is influenced by space–energy effects, it is considered convenient to introduce a reference power spectral density (PSD) yielding space-independent results, and to express the $CPSD_R$ relatively to this quantity.

$$\xi(\mathbf{x}_1, \mathbf{x}_2, \omega) = \frac{|\mathrm{CPSD}_R(\mathbf{x}_1, \mathbf{x}_2, \omega)|}{\mathrm{PSD}(\omega)}, \tag{18}$$

ξ represents the relative magnitude of the $CPSD_R$ and may be normalized to 1 at a suitable low-frequency point (e.g. in the plateau region of the reactivity transfer function) for the given detector locations.

There are several possibilities for defining a reference PSD:

A first-reference PSD can be established by first-order approximation of the kinetics of our reflected system to those of an equivalent bare system with detectors uniformly distributed through the core. This bare-reactor equivalent CPSD, which will be denoted by PSD_P, has the spectral shape (see also Appendix C) when we include for completeness the small feedback effect of the delayed neutrons appearing in the noise-equivalent source term of equation (16):

$$\mathrm{PSD}_P \sim |1-h|^2 |G|^2 \tag{19}$$

In equation (19), G is the familiar point-reactor reactivity transfer function.

$$G = \frac{1}{j\omega\Lambda + h - \rho}, \tag{20a}$$

where A is the neutron generation time and ρ the reactivity.

Equation (20a) becomes in the prompt-neutron approximation $\left(\omega > \frac{1}{\lambda_i}\right)$:

$$G \cong \frac{1}{\Lambda(j\omega + \alpha)} \tag{20b}$$

$\alpha = (\beta - \rho)/\Lambda$ is the prompt-neutron decay-time constant of the fundamental prompt-period mode. The use of equation (19) as reference requires the determination of Λ (as an overall quantity of the system) or an α-search, respectively.

An alternative reference is the APSD of the reactor power when we fictitiously apply small random reactivity perturbations to the unperturbed stationary reactor system. This second-reference case can be formulated independently of the α-concept. There are still other reference concepts possible, e.g. to use the $CPSD_R$ of detectors completely distributed through the reflected-reactor system. This case will be discussed in Section 6.

4.1. α-Search

Following the paper of Preskitt *et al.* (1967), we seek solutions to the reactor kinetic equations which vary exponentially in time after instantaneous removal of the extraneous source from the stationary subcritical reactor system at the time point $t = 0$.

$$\phi_{1n}(\mathbf{x}, t) = \psi_{1n}(\mathbf{x})\, e^{\omega_n t} \tag{21a}$$

$$\phi_{2n}(\mathbf{x}, t) = \psi_{2n}(\mathbf{x})\, e^{\omega_n t} \tag{21b}$$

$$C_{in}(\mathbf{x}, t) = c_{in}(\mathbf{x})\, e^{\omega_n t} \tag{21c}$$

If these vectors are substituted into the source-free kinetic equations (1a–c) and the precursor densities are eliminated, we obtain the system of ω- or period-eigenfunctions:

$$\begin{pmatrix} \mathrm{div}\, D_1\, \mathrm{grad} - \Sigma_1, & \nu\Sigma_f(1-h_n) \\ \Sigma_R, & \mathrm{div}\, D_2\, \mathrm{grad} - \Sigma_2 \end{pmatrix} \begin{pmatrix} \psi_{1n} \\ \psi_{2n} \end{pmatrix} = \omega_n \begin{pmatrix} \frac{1}{v_1}\psi_{1n} \\ \frac{1}{v_2}\psi_{2n} \end{pmatrix}, \tag{22}$$

with the abbreviation

$$h_n = \omega_n \sum_i \frac{\beta_i}{\lambda_i + \omega_n}.$$

Equation (22) is the general expression to be satisfied by all exponentially-varying solutions to the reactor kinetic equations and evidently does not contain any reference to the reactivity of the system.

According to the conventional reactivity concept, the reactivity defined as $\rho = (k-1)/k$ (where k is the effective multiplication factor in the static reactor) is the algebraically-largest eigenvalue resulting from the static multiplication eigenfunction equation

$$\begin{pmatrix} \mathrm{div}\, D_1\, \mathrm{grad} - \Sigma_1, & \nu\Sigma_f(1-\rho) \\ \Sigma_R, & \mathrm{div}\, D_2\, \mathrm{grad} - \Sigma_2 \end{pmatrix} \begin{pmatrix} \varphi_1 \\ \varphi_2 \end{pmatrix} = 0. \tag{23}$$

Writing the adjoint functions φ_1^+, φ_2^+ of equation (23) and using the definition of adjoint operators allow the elimination of the loss operators since these are common to equations (22) and (23). The result is a generalized inhour equation,

$$\rho = \omega_n \left[\frac{\int dV \left(\frac{1}{v_1} \varphi_1^+ \psi_{1n} + \frac{1}{v_2} \varphi_2^+ \psi_{2n} \right)}{\int dV \varphi_1^+ \nu\Sigma_f \psi_{2n}} + \sum_i \frac{\beta_i}{\lambda_i + \omega_n} \right], \tag{24}$$

in which we can identify the neutron generation times for the spectrum of the (fundamental) kinetic modes satisfying equation (24) by

$$\Lambda_n = \frac{\int dV \left(\frac{1}{v_1} \varphi_1^+ \psi_{1n} + \frac{1}{v_2} \varphi_2^+ \psi_{2n} \right)}{\int dV \varphi_1^+ \nu\Sigma_f \psi_{2n}}. \tag{25}$$

All the roots ω_n have negative values. The prompt decay-time constant α in equation (20b) is equal to the largest negative eigenvalue belonging to the subset of eigenvalues and corresponding kinetic modes which can satisfy equation (24). If Λ is the prompt-neutron generation time corresponding to the eigenvalue $-\alpha$, equation (24) results to a high approximation in the well-known relationship

$$\rho = -\alpha\Lambda + \beta. \tag{26}$$

In the numerical investigation of our reflected-reactor model we have followed the generally-convenient concept of generating subcritical states by fuel manipulation, i.e. simply by setting $\nu\Sigma_f = k(\nu\Sigma_f)_{cr}$ where $(\nu\Sigma_f)_{cr}$ is the fission cross section used previously in a criticality calculation to establish the critical dimension of the system. Since in this procedure ρ and β were known quantities, α was determined by solving equation (22) and Λ resulted then from equation (26). The eigenvalue equation for the ω_n can formally be written very similarly to the static eigenvalue equation (A.9) of Appendix A. However, equation (25) was used as a cross-check. A further check was that the prompt-neutron lifetime should remain invariant while the reactivity state of the previously-defined critical system was changed by fuel manipulation.

4.2. PSD of power fluctuations induced by random reactivity fluctuations

We perturb fictitiously the stationary reactor system by small stochastic reactivity fluctuations $\delta\rho(t)$ with the expected value $\langle \delta\rho(t) \rangle = 0$. These reactivity fluctuations expressed in the frequency domain appear in the input signal δS_1 of equation (10) as

$$\delta S_1 = -(1-h)\nu\Sigma_f \phi_2 \delta\rho. \tag{27}$$

This signal δS_1 produces, at a space point $\mathbf{x}_1$, fluctuations of the thermal-neutron flux which follow from the application of equation (5) when we formally set the detection cross-section $\Sigma_{1d} = 0$ and $\Sigma_{2d} = 1$, and correspondingly redefine the system of kinetic importance functions given by equations (8). We will denote these functions by $\phi_1'^+, \phi_2'^+$. We obtain then, for the thermal-flux fluctuations,

$$\delta\phi_2(\mathbf{x}_1, \omega) = -(1-h)\delta\rho(\omega) \int dV \phi_1'^+(\mathbf{x}, \mathbf{x}_1, \omega)\nu\Sigma_f(\mathbf{x})\phi_2(\mathbf{x}). \tag{28}$$

The frequency spectrum of the reactor power fluctuations follows from

$$\delta P(\omega) = C \int dV_1 \Sigma_f(\mathbf{x}_1)\delta\phi_2(\mathbf{x}_1), \tag{29}$$

C is a conversion constant. Substituting equation (28) into equation (29) yields

$$\delta P(\omega) = (1-h)G_{PF}(\omega)\delta\rho(\omega), \tag{30}$$

where G_{PF} is a transfer function given by

$$G_{PF}(\omega) = C \int\int dV_1 \, dV \Sigma_f(\mathbf{x}_1)\phi_1'^+(\mathbf{x}, \mathbf{x}_1, \omega)\nu\Sigma_f(\mathbf{x})\phi_2(\mathbf{x}). \tag{31}$$

The power spectral density, PSD_{PF}, of the reactor power fluctuations follows then from

$$PSD_{PF} = |1-h|^2 \, |G_{PF}|^2 PSD_\rho, \tag{32}$$

PSD_ρ denotes the PSD of the input reactivity fluctuations. It is to be noted that in writing equation (32) we factored out the small delayed-neutron effect $|1-h|^2$, so that this term appears as a common factor between the $CPSD_R$ and PSD_{PF} and the previously-defined reference PSD_P, and is cancelled in ξ.

With a white-noise assumption for the reactivity fluctuations, equation (32) establishes another possibility for a reference PSD. In the first-reference case (PSD_P of equation (19)) only the contribution of the prompt fundamental mode is considered, while in this second-reference case (PSD_{PF} of equation (32)) the closed solution of $\phi_1'^+$ contains implicitly all kinetic modes, and therefore also completely the neutronic feedback of the reflector to the core.

In the numerical evaluation we have found differences in the spectral shapes between the PSD_P and PSD_{PF} in our reflected model. Small, but negligible differences (of the order of a few percent) were observed

at higher frequencies (toward the end of the considered frequency range of 400 Hz) in the case of a light-water-moderated core with a light-water reflector. The moderator and the reflector have here the same nuclear properties. For this reason, we generally used the simpler reference concept of the PSD_P. If, however, one replaces the light-water reflector by a heavily-reflecting one (such as D_2O or graphite) one finds significant deviations due to the expected distortion by higher kinetic modes. These also occur at low frequencies where the delayed-neutron contribution becomes important.* In the next section we will give a summary of the experimental investigations before proceeding to the numerical results of the model evaluation.

5. SUMMARY OF THE EXPERIMENTAL INVESTIGATIONS

Neutron-noise analysis with various two-detector arrangements in the reflector zone was performed on the reactor SAPHIR in the time domain as well as in the frequency domain. The zero-crossing correlation technique is an on-line method in the time domain and uses a polarity correlator. Under the assumption of the applicability of the point-kinetics model the zero-crossing point of the polarity cross-correlation function is primarily related to the prompt-neutron decay constant α. When, in a calibration measurement, the prompt-neutron decay constant α_c at delayed critical is determined, the reactivity can be obtained for subcritical states down to about -5 \$. For more subcritical states the method becomes insensitive. If significant spatial effects are present, invalidating the application of the point-kinetics model, the method does not give a direct indication of such effects. To obtain more detailed information cross-power spectra were simultaneously measured. The cross-power spectra were compared to the spectral shape resulting from the point-kinetics model. An independent value of the reactivity was obtained using the rod-drop method.

In the experiments, the detectors were highly-efficient ionization chambers filled with ^3He.† The active length (40 cm) ensured a good flux integration over the core height (60 cm). The collector electrode was connected via an 8-m long cable to the low-impedance input of a current amplifier stage at virtual ground, whereas negative high tension from a battery was applied to the chamber box. Each chamber was completely shielded with a ground connection separated from the reactor mass. This procedure prevented any appreciable pick-up of the 50 Hz mains hum, the frequency of which lies inside the required frequency range. The chamber setup was placed in a waterproof guiding tube (i.d. 7 cm) and well centred in it at the reactor mid-plane. Each guiding tube had a rigid extension (about 1 m long) with ceramic isolated wires to give further protection of the cables from radiation damage. The guiding tubes were always inserted in free lattice positions outside the core adjacent to a fuel element.

For the application of the zero-crossing correlation method, the noise signal from each detector was amplified by a recently-improved amplifier system with automatic d.c.-offset, input sensitivity control and gain control of the post-amplifier stage following signal filtering, to keep the output signal r.m.s. at a constant level of 1 V independently of the reactor flux conditions. The latter was a desirable feature with regard to the small inherent hysteresis of the signum generators in the polarity correlator. The polarity correlator is a completely digital device and contains a feedback to the delay path in one channel for an automatic search for the zero-crossing point τ_0 of the polarity cross-correlation function. For the theoretical background, and a block-diagram of the equipment, reference is made to the paper of Behringer and Peier (1979). Instantaneous values of the meter display (proportional to τ_0) can periodically be read out on paper tape, allowing in particular an estimate of the display variance. Another available signal provides for the output of display values which represent time-averages during each read-out period.

The signal conditioners in both measuring channels were well matched. Each band-pass filter consists of a single RC high-pass filter and double RC low-pass filter. They were adjusted in each channel to $\omega_L/2\pi = 15$ Hz (3 dB low frequency cut-off) and $\omega_H/2\pi = 200$ Hz (effective 3 dB high frequency cut-off). The zero-crossing correlation method requires a frequency range to be set $\omega_L \lesssim \alpha(\rho) < \omega_H$. The high-pass filter is responsible for the generation of the zero-crossing point while the low-pass filter cuts the detection-noise component in each channel. This component does not affect τ_0, but its variance, and is a necessary prerequisite for the generation of well-defined signum signals. Moreover, this low-pass filter is expected to reduce correlated high-frequency noise components which are

* We will not represent these findings by plots, because we prefer to restrict the investigations to a light-water-moderated core with a light-water reflector.

† The ^3He detectors were specially manufactured by the Laboratory Professor Berthold. D-7547 Wildbad/Schwarzwald, Germany. The active volume was 40 cm in length and 4 cm in diameter. It was filled with 99% guaranteed ^3He at a pressure of 5 bar without addition of any quenching gas. The inner collector electrode consisted of a small tube to ensure operation in the ionization range. For dealing with detector currents of the order of several μA under saturation condition a high tension of 1600 V was required.

due to space effects, and to make the point-reactor model applicable to a good approximation.

The filter parameters enter into the relation between α and τ_0. Filter characteristics can be measured very accurately, so that the presence of systematic errors, in this connection can be practically excluded. An experimental check on the overall-performance of the meter does not require a reactor. The noise sources can be simulated by three independent white-noise generators. This technique (explained in the paper of Behringer and Peier (1979)) was used not only for a periodical check of the equipment performance but also for the verification of the display variance behaviour as theoretically predicted. For the spectrum measurements, broad-band noise signals (0.1 Hz–1 kHz) were taken from each amplifier channel and fed to the dual channel Fast Fourier Transform Analyzer OMNIFEROUS FFT 400B (Nicolet Scientific Corp.) or to a magnetic tape for post-analysis.

First experimental checks showed that an excore detector arrangement gives sufficient detector efficiencies to obtain the required information within reasonable measuring times. Assuming the validity of the point-reactor model, and approximately equal detector efficiencies in the selected positions, an estimate of the so-called reduced detector efficiency can be obtained either from the slope of the polarity cross-correlation function at τ_0,* or from a coherence function measurement at a frequency $\omega = \alpha_c$ when the reactor is made critical. The reduced detector efficiency is defined by Behringer and Peier (1979) as

$$Q = \frac{f W \mathrm{D}}{\mathrm{B}} \tag{33}$$

W = detector efficiency in unit counts per fission in the system

B = Bennet factor, with B defined as $\overline{q^2}/\bar{q}^2$, where q is the charge released per detected neutron

D = Diven factor

f = spatial correction factor, of order unity, depending on reactor geometry and spatial fission-rate distribution.

The results given by the two methods were not in good agreement. However, the values Q obtained under critical-reactor conditions varied between $(1\text{–}4) \times 10^{-3}$ indicating a very high detector efficiency. Since a detector may have a non-negligible but unknown sensitivity to γ's, it is felt that Q need not be a constant (for unchanged detector positions) when, in subcritical states, the γ-background becomes more important. Systematic investigations performed on different core configurations with varied and sometimes widely-separated detector positions around the core (excluding the region of the Be-reflector) yielded reasonable consistency between α-values given by the zero-crossing correlation method and those evaluated from the magnitude of the cross-power spectra. In the considered frequency range up to 500 Hz, the CPSD always showed zero-phase behaviour.

For the evaluation of the cross-power spectra, the $\mathrm{PSD_P}$ of equation (19) was used as reference, and α was varied until the fit gave a horizontal line for ξ of equation (18) in a frequency range from about 5 to about 100–150 Hz. In the measurements any forced coolant flow had to be avoided. Manual control of the reactor was used for measurements in the critical reactor state. α-determinations with various detector positions in the same core configurations gave the same result within the experimental accuracy. Reactivity determinations via equation (26) using the previously-measured α_c-value agreed well, in most cases, with values obtained by the rod-drop method, strongly suggesting that the use of point kinetics is a valid approach. As an example Fig. 2 shows a core

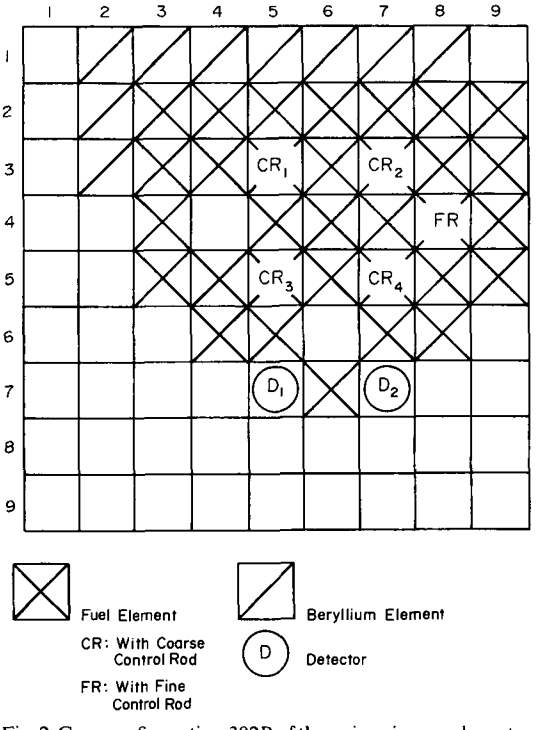

Fig. 2. Core configuration 392B of the swimming-pool reactor SAPHIR with indication of the detector positions (lattice size: 81 × 77 mm).

* This slope could be measured by a special feature included in the design of the polarity correlator. By disturbing the integrator (forward–backward scaler) in one direction with a well-defined external pulse rate, τ_0 could be shifted.

configuration (392B) in which several measurements have been made. This core configuration represents a rather unfavourable case. There is a fuel element between the detector positions and nearby an empty lattice place (reserved for isotope production) and coarse control rods. Significant flux perturbations were therefore expected in this core region. Results are given in Table 1.

The rod-drop method for the determination of subcritical reactivities is a routine procedure on SAPHIR. The neutron-flux decay after a rod-drop is measured by a high-resolution counting channel equipped with a fission counter. It processes pulse-rates up to 10^7 cps with dead-time losses of about 12% at that counting rate. This device, which was developed by Behringer and Phildius (1974), enables measurement of the flux decay over several decades and is insensitive to the γ-background. The evaluation method developed by Demarmels (1968) is based on a modified technique using the modal approach with kinetic eigenfunctions and the elimination of the prompt harmonics and the kinetic distortion. The photoneutrons produced in the Be-reflector are not considered in the code. As pointed out by Cohn (1959), they can give rise to transients which could introduce appreciable errors in the reactivity determination. Since the Be-reflector used in SAPHIR covers only a part of the core, it appears, according to previous experience, that this photo-neutron effect should give only a negligible perturbation. The errors given in Table 1 represent overestimates in the case of the results from the noise method, whereas they are purely statistical for the rod-drop results.

In the core configuration shown in Fig. 2, an on-line measurement of the time evolution of the xenon poisoning after a shutdown from a steady power operation was performed. The results of this measurement will be reported separately. They give further indication of the applicability of the point-reactor model. The evaluation of this measurement allowed an estimate to be made of the core-average thermal flux at power and the equilibrium xenon reactivity worth and, in addition, an independent but indirect determination of α_c. The latter measurement gave a value of $\alpha_c = 114 \pm 2$ rad/s, which is in excellent agreement with the other results given in Table 1. Koehler (1980) recently began a calculation of α_c for this core configuration under the actual burnup conditions of the fuel elements. His very preliminary result obtained by this calculation using a 2-D code is $\alpha_c = 129.6$ rad/s. This value seems to be somewhat too high, but is of the same order as the experimental data.

Two typical experimental cross-power spectra from about 2.5 to 500 Hz, represented by the quantity ξ of equation (18) with varied values of α, are shown in Figs 3 and 4. Figure 3 refers to the case of a very nearly critical reactor state (reactor power ~ 500 W), and Fig. 4 to the case of a subcritical state with $\rho = -3.7$ \$. The measuring time was 30 min in both cases. The curves are normalized around 10 Hz and slightly band-pass corrected in the higher-frequency region. In the lower-frequency region which is larger in the subcritical case due to the more extended plateau in the reactivity transfer function, ξ can be brought practically to a horizontal line by a proper adjustment of α. This suggests (but does not confirm) that this lower-frequency region may be regarded as the validity range of the point-reactor model. At higher frequencies, where statistics become inadequate due to the rapidly-decreasing coherence, ξ increases significantly with frequency. This behaviour, which is less pronounced in the subcritical state, indicates that the measured cross-

Table 1. Measured values of the prompt-neutron decay constant α and the reactivity ρ at core configuration 392B

Detector locations	Coarse control rod positions (mm)				Prompt neutron decay constant (rad/s) obtained from		Reactivity (−\$)		Remarks
	CR_1	CR_2	CR_3	CR_4	Polarity CCF	CPSD	Noise method (polarity CCF)	Rod-drop method	
75/77	283	283	283	283	115±4				Critical power 5 kW
75/77	0	281	281	281	220±7	225±5	0.91±0.09	0.923±0.0015	
75/77	0	281	0	281	540±32	555±20	3.70±0.32	3.62±0.03	
75/77	0	0	0	0	745±58		5.48±0.55	5.24±0.08	
74/78	276	276	276	276	115±4	115±3			Critical power 5 kW
74/78	0	0	0	0	702±53		5.10±0.51	5.11±0.06	

CR-positions: 600 = upper limit; 0 = lower limit.

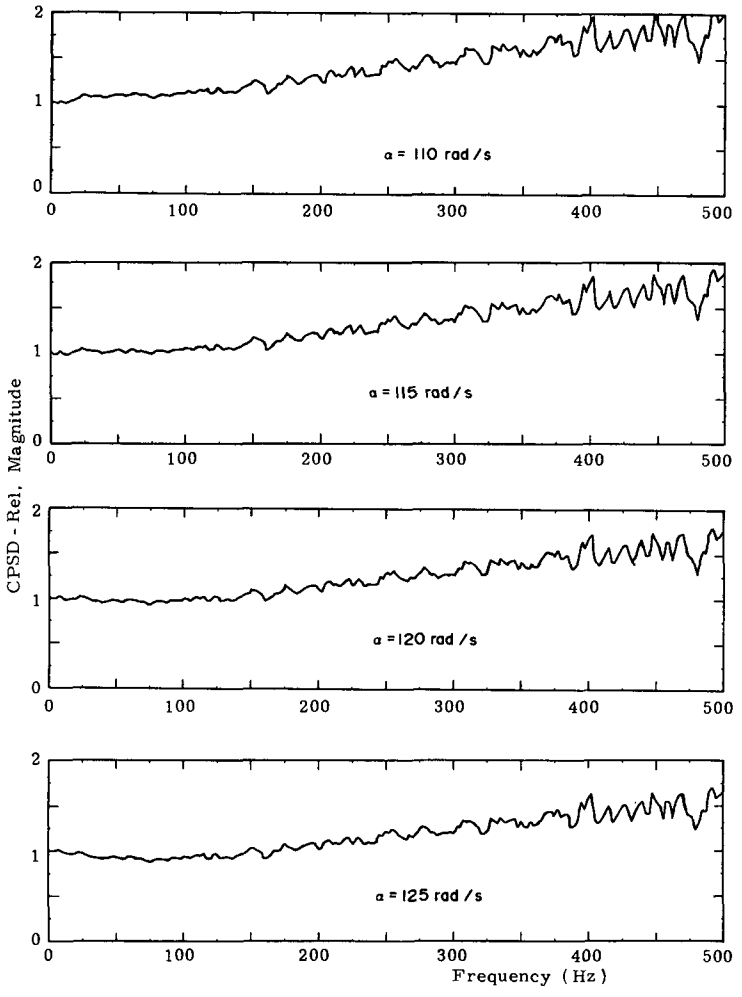

Fig. 3. A typical cross-power spectrum measured in a nearly critical reactor state and represented relative to the point kinetic CPSD with varied values of the break frequency.

power spectra decrease less strongly than predicted by the point-reactor model. This trend was generally found in all cross-power spectra measurements with excore detector locations varied around the core. Before discussing this result further we shall consider, in the next section, the numerical results of our model calculation and put the question whether this trend observed in the experimental investigations can be reproduced by our simple model.

6. NUMERICAL RESULTS OF THE MODEL CALCULATION

For the appearance of space effects, an important parameter is the core-size H. In a bare homogeneous reactor, space effects are negligible up to moderate frequencies, i.e. up to frequencies which may not be higher than several times the break frequency α_c,* if

$$H \ll \frac{\pi M}{\sqrt{\beta}}, \tag{34}$$

where M = migration length and β = effective fraction of delayed neutrons, and the detectors are not too close to the core boundaries. The importance of the inequality (34) is explained in Appendix C. A reactor system which satisfies the inequality (34) may be called a small one. Unfortunately, there is no further criterion available for specifying how well this inequality should

* This statement is not valid in the case of a perturbation propagating through the core, like the two-phase coolant flow in a BWR (Behringer *et al.* (1979)).

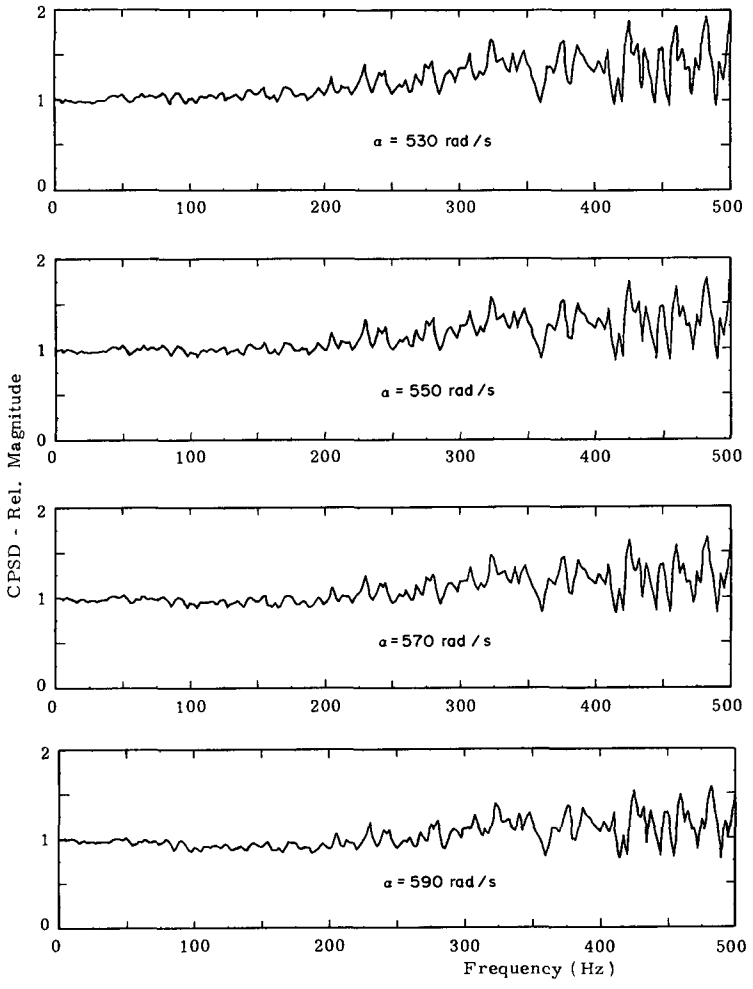

Fig. 4. A typical cross-power spectrum measured in a subcritical state at -3.7 \$ and represented relative to the point kinetic CPSD with varied values of the break frequency.

be satisfied by a small system. For a small equivalent system which is reflected, the reflector saving is normally relatively high. Core- and reflector-kinetics must, therefore, be coupled rather strongly. Up to this point, the appearance of space effects is not governed by the core-size, H, alone, but also by the nuclear properties of the reflector material.

The r.h.s. of the inequality (34) is of the order of 2.5 m for an LWR. Power-LWRs have typical core sizes of this order of magnitude. Thus, one should not speak of large systems, but rather of systems of intermediate size. Nevertheless, we will follow the usual concept and speak of a large system in this case. A reflector on such a system has little influence on incore measurements. But, in any case, the core kinetics start to become space dependent.

In the numerical calculation we used group parameters that are typical for a highly-enriched uranium-water lattice and a light-water reflector. The data are given in Table 2 (Winkler and Koehler, 1975). They were selected for a rather high burnup ($\sim 50\%$). In this case we reached a critical core-size, $H = 77.6$ cm, and an α_c-value of 122 rad/s (with $\beta = 7 \times 10^{-3}$). These figures are representative for the reactor SAPHIR in an advanced burnup condition and are believed to be close to the actual conditions under which the experimental investigations have been performed. Since, with regard to the inequality (34), this core size cannot be regarded as small, we call this model a realistic system.

In order to get deeper insight into the trends of the spatial effects, a large system with $H = 197$ cm was also considered. It was created by adjustment of the thermal

Table 2. Two-group parameters used in the model calculation

	Core		H_2O reflector
D_1 (cm)	1.441		1.152
D_2	2.848×10^{-1}		1.652×10^{-1}
Σ_{a1} (cm^{-1})	2.742×10^{-3}		4.876×10^{-4}
Σ_{a2}*	7.680×10^{-2}	for $H = 77.6$ cm	1.780×10^{-2}
	8.110×10^{-2}	for $H = 197$ cm	
Σ_R	2.718×10^{-2}		5.166×10^{-2}
$\nu\Sigma_f$	9.360×10^{-2}		
v_1 (cm/s)		5.304×10^7	
v_2		2.482×10^5	

* Adjusted correspondingly to the models and different core sizes to obtain criticality.

absorption and had an α_c-value of about 130 rad/s. The same procedure of adjusting the thermal absorption was used for performing comparison calculations for a bare-reactor model.

As mentioned in Section 4.1, subcritical states were generated by fuel manipulation. We confine the representation of the results obtained in the frequency domain to two states, the critical state and a subcritical state at -5 \$. With regard to a few calculations extended to very low frequencies (see Fig. C1) the usual six groups of delayed neutrons were generally taken into account. The detectors were assumed to be sensitive to thermal neutrons only.

A useful quantity for characterizing the togetherness of the detected neutron-noise field, or the coupling between regions being sampled by the detectors, is the coherence function (Albrecht and Seifritz, 1968). We define it here by

$$\mathrm{COH}(\mathbf{x}_1, \mathbf{x}_2, \omega) = \frac{|\mathrm{CPSD}_R(\mathbf{x}_1, \mathbf{x}_2, \omega)|}{\sqrt{[\mathrm{CPSD}_R(\mathbf{x}_1, \mathbf{x}_1, \omega) \cdot \mathrm{CPSD}_R(\mathbf{x}_2, \mathbf{x}_2, \omega)]}} \quad (35)$$

6.1. Both detectors located in the core

Figure 5 shows first the case where relative CPSD_Rs, i.e. the quantity ξ defined by equation (18), are plotted

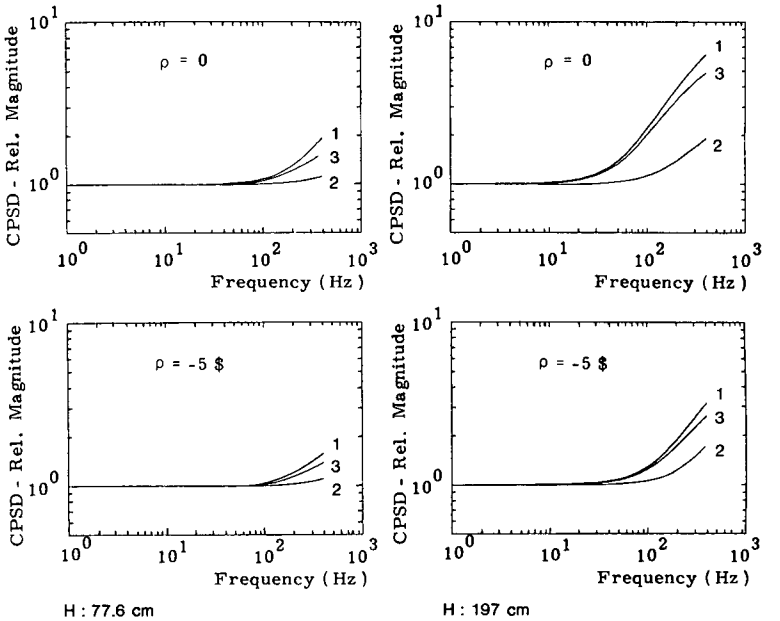

Fig. 5. Relative CPSDs of incore detectors at different common positions. The upper figures refer to the critical state, the lower figures to a subcritical state at -5 \$. Curve 1: detector position $\mathbf{x}_1 = \mathbf{x}_2 = 0.10 \times H$; curve 2: detector position $\mathbf{x}_1 = \mathbf{x}_2 = 0.50 \times H$; curve 3: detector position $\mathbf{x}_1 = \mathbf{x}_2 = 0.90 \times H$.

for different detector positions in the core when both detectors are located at the same point (or are always very close together). In this, and all following figures representing relative magnitudes of the $CPSD_R$, ξ has been normalized to equal 1 at 1 Hz. The frequency range considered extends from 1 to 400 Hz. One recognizes the general trend, that at higher frequencies the $CPSD_R$s roll-off less strongly than predicted by the point model. The onset and increase of the spatial effects with increasing frequency are obviously more pronounced for the large system than for the realistic system, and for coincident detector positions near the core boundaries. Due to the asymmetry of the reflected model, the deviation from the PSD_P is somewhat less for a detector position nearer the reflector side (curve 3) than for a position near the free core boundary and symmetrically placed with respect to the core centre (curve 1). There must be a position in the vicinity of the core centre where the magnitude of the space effects is minimized (in a bare homogeneous reactor, this point is exactly the core centre where the first prompt harmonic vanishes). The space dependence appears less pronounced and its onset is shifted to somewhat higher frequencies in the subcritical state than in the critical state due to the competing longer plateau region of the reactivity transfer function. Calculations performed e.g. by Sheff and Albrecht (1966b) and Natelson *et al.* (1966) on a bare reactor, and by Sheff (1968), who included the case of a reflected system, show similar results.

The general behaviour of the $CPSD_R$s in Fig. 5 can be understood by considering, that it should asymptotically approach the infinite medium form at high frequencies. This form is given in Appendix C. Using equation (C.21), the frequency dependence of ξ results in

$$\xi(\mathbf{x}_1 = \mathbf{x}_2, \omega) \sim \sqrt{\left[\frac{\omega^2+\alpha^2}{\alpha+\sqrt{(\omega^2+\alpha^2)}}\right]}. \qquad (36)$$

Equation (36) represents a very rough approximation, but nevertheless exhibits the main characteristics of the trend.

The situation appears to be different when one considers detectors at separate positions in the core. Figure 6 shows $CPSD_R$s (relative magnitude and phase) and coherence functions in the critical state for the realistic system, whereas Fig. 7 represents results in the subcritical state. Results corresponding to the large system are shown in Figs 8 and 9. There are again cases where, in the higher frequency range, the magnitude of the $CPSD_R$ decreases less strongly with increasing frequency than the PSD_P, but there are more recent cases showing an opposite behaviour. It seems that these characteristics are related to the first prompt

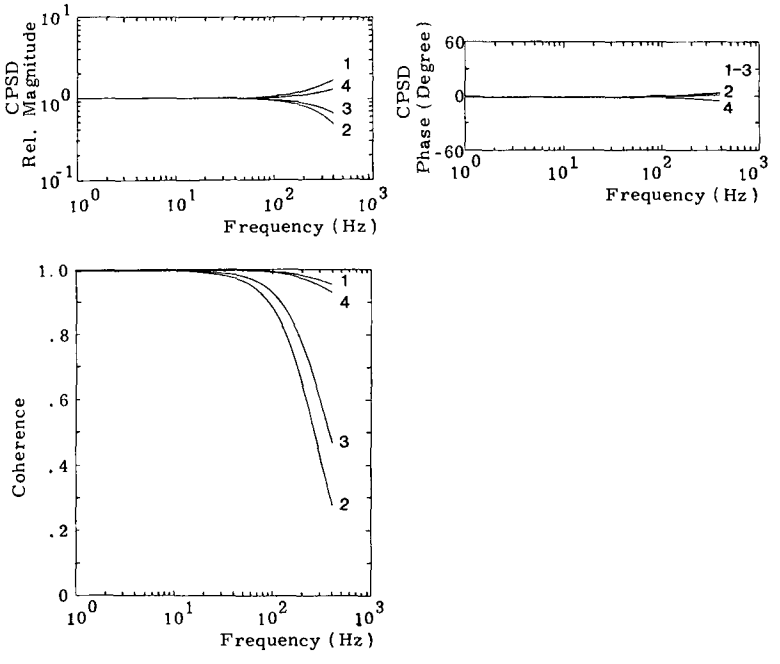

Fig. 6. Relative CPSDs and coherence functions of incore detectors at different separated positions in the critical state for $H = 77.6$ cm. Curve 1: detector position $\mathbf{x}_1 = 0.10 \times H$, $\mathbf{x}_2 = 0.25 \times H$; curve 2: detector position $\mathbf{x}_1 = 0.10 \times H$, $\mathbf{x}_2 = 0.90 \times H$; curve 3: detector position $\mathbf{x}_1 = 0.25 \times H$, $\mathbf{x}_2 = 0.75 \times H$; curve 4: detector position $\mathbf{x}_1 = 0.75 \times H$, $\mathbf{x}_2 = 0.90 \times H$.

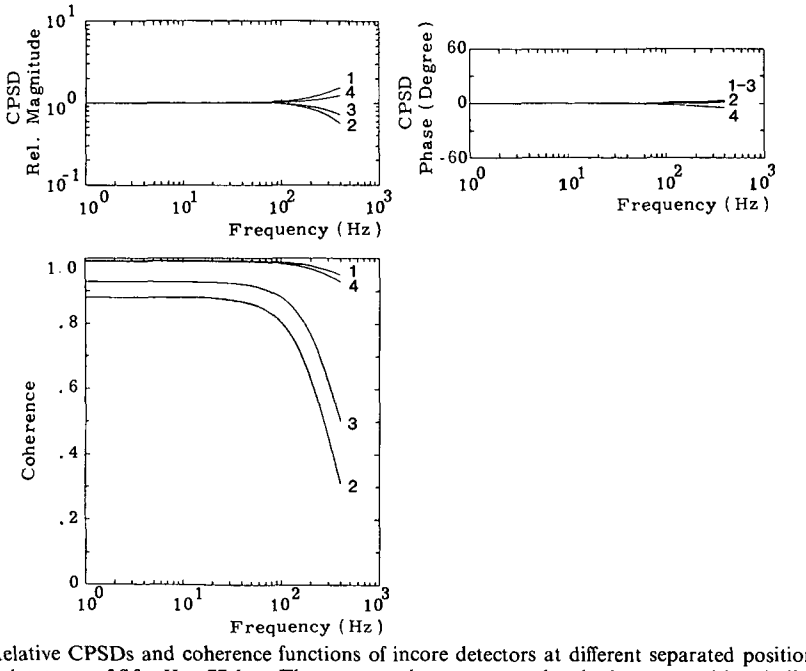

Fig. 7. Relative CPSDs and coherence functions of incore detectors at different separated positions in a subcritical state at $-5\$$ for $H = 77.6$ cm. The curve numbers correspond to the detector positions indicated in Fig. 6.

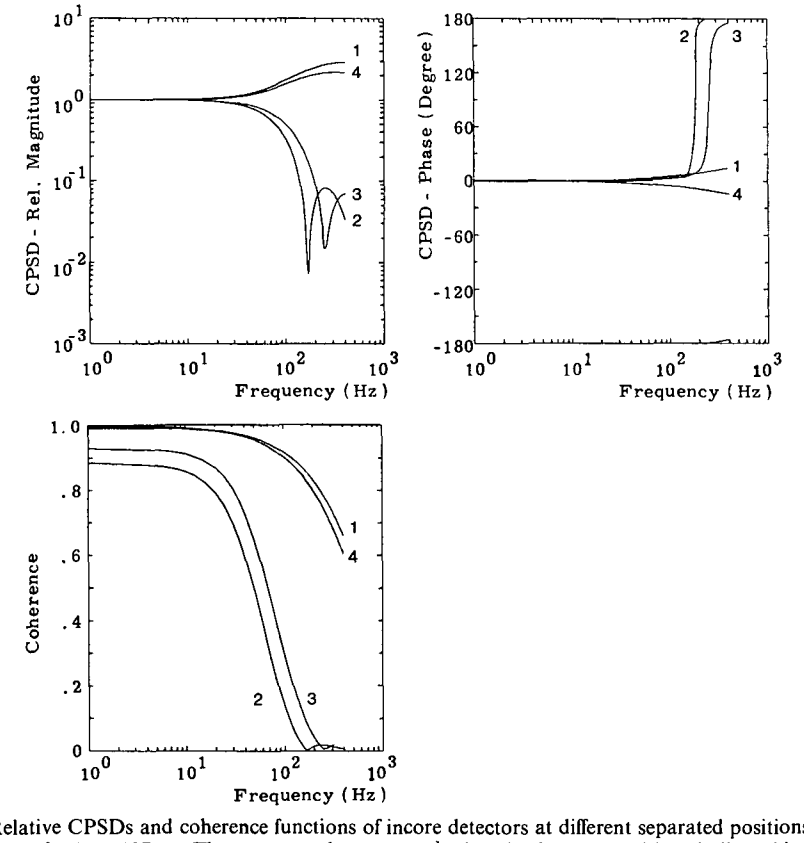

Fig. 8. Relative CPSDs and coherence functions of incore detectors at different separated positions in the critical state for $H = 197$ cm. The curve numbers correspond to the detector positions indicated in Fig. 6.

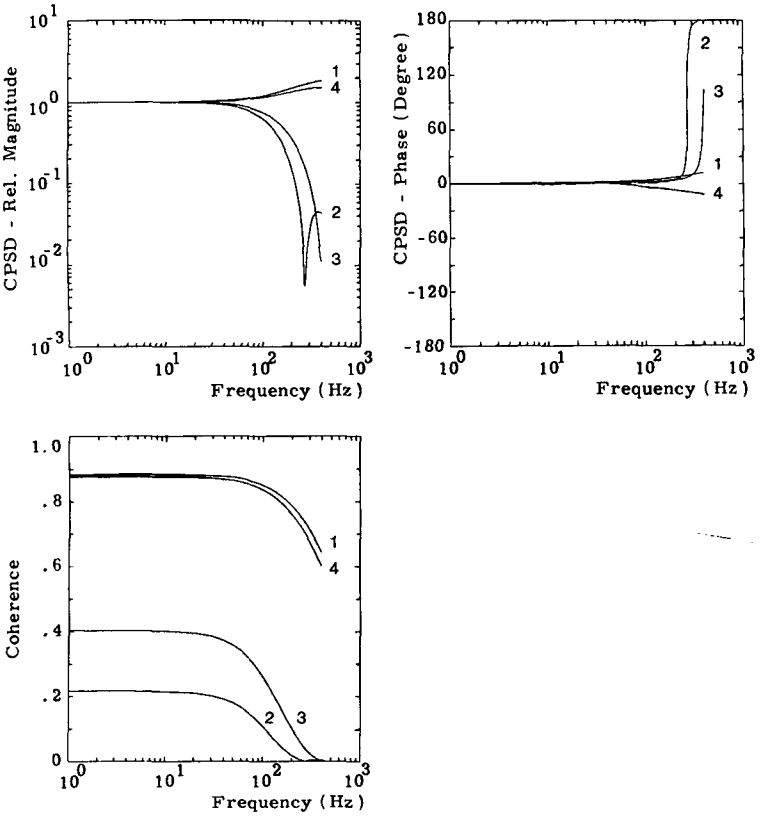

Fig. 9. Relative CPSDs and coherence functions of incore detectors at different separated positions in a subcritical state at $-5\$$ for $H = 197$ cm. The curve numbers correspond to the detector positions indicated in Fig. 6.

harmonic mode and depend on whether it has equal or opposite sign at the space points considered.

It should be noted that the effect of a decrease of ξ with frequency was experimentally observed on the reactor SAPHIR in a measurement where the ^{3}He chambers could be installed at two different empty lattice positions provided for isotope production. However, a clear interpretation of the result cannot be given due to the irregular core configuration, the unknown flux perturbations introduced by the detectors and control rods in the vicinity and the impossibility of making check measurements in other incore locations.

For detectors widely spaced in the large-core model unusual behaviour of the CPSD_R or coherence function, respectively, can be observed. A sink appears at a particular frequency. There are further sinks at higher frequencies not shown in the figures. At these sink frequencies a sign change of the real part of the CPSD_R occurs, leading also to a phase jump, and the CPSD_R becomes purely imaginary. The values of the sink frequencies increase with increasing subcriticality and decreasing detector distance. The possible appearance of a sink structure is well known in coupled-core kinetics and has been experimentally verified (Hendrickson and Danofski, 1967; Albrecht and Seifritz, 1968; Seifritz and Albrecht, 1968; Ebert *et al.*, 1974a,b; Viehl, 1975; Genoud, 1977; Morishima, 1979; Nagy *et al.*, 1979). It is an interesting feature that such a structure can also appear in our continuous model. The physical reason for sink frequencies is a certain cancellation of stochastic fluctuations at a particular frequency of cross-correlation due to neutrons arriving at the detectors with cancelling phase relationships caused by spatial effects (Albrecht and Danofski, 1969). Using the picture of the infinite medium approach (see Appendix C), widely-separated detectors sample from different, not completely common regions of the neutron field. This is manifested by the relatively bad coherence at low frequencies in Figs 8 and 9. If we disregard the influence of the reflector and consider for simplicity the case of widely- and symmetrically-spaced detectors in a large bare homogeneous reactor, the system approaches a coupled symmetrical two-spatial

node model. Each node contains an independent driving source with the same statistical property, and is fedback by the other node through a transfer function characterizing the transit of neutrons with a delay time (or a delay-time distribution). Albrecht and Seifritz (1968) showed, that such a system must have at least one sink frequency in the coherence function. This sink frequency is shifted to higher values with increasing subcriticality.

The space-dependent characteristics of the $CPSD_R$ shown for detector positions in the core are not typical for the reflected system, except when a detector is located near to the core–reflector interface. A light-water reflector is in principle a bad reflector which does not significantly influence the kinetics of the light-water-moderated core. This follows from a comparison study on the bare homogeneous reactor model (in two groups). Very similar characteristics resulted, and in addition the sink structure for widely-spaced detectors in a large system was found. These calculations were performed in two ways, using the closed solution of the kinetic importance functions, and the method of modal expansion. Both procedures led to the same results.

6.2. *One detector in the core, second detector in the reflector*

Plots are given in our EIR-report 446 (1981), when one detector is located at various positions in the core, whereas the other detector is located at the position of the thermal flux peak in the reflector. The characteristics are similar to the case when both detectors are incore. There is no significant difference. When the detector spacing is large in the large system, the sink structure appears again.

Robinson and Alexander (1971) reported on a calculation showing a break frequency behaviour in the imaginary part of the $CPSD_R$ in the vicinity of 500 Hz for detector distances of 9.8 and 15.9 cm. This behaviour is not predicted by nodal models, but was found in measurements at ORNL. When we plotted the imaginary part of the $CPSD_R$ referring to the realistic system, we found very similar curves. The onset of this break behaviour shifts to lower frequencies with increasing detector distance. In our calculations, it began at about 100 Hz for an incore detector position at $x_1 = 0.1 \times H$ (detector distance about 72 cm). Thus, we conclude, that our simple space-dependent model contains all the essential information.

6.3. *Both detectors located in the reflector zone*

Spatial effects in the reflector zone have been studied for detector positions around the region of the thermal flux peak. Positions far away from the core–reflector interface are not of interest because the noise is dying out in these regions.

Figure 10 shows results obtained for the relative $CPSD_R$s. In the frequency range under consideration the curves again show a roll-off at higher frequencies, which is weaker than given by the PSD_P. The behaviour

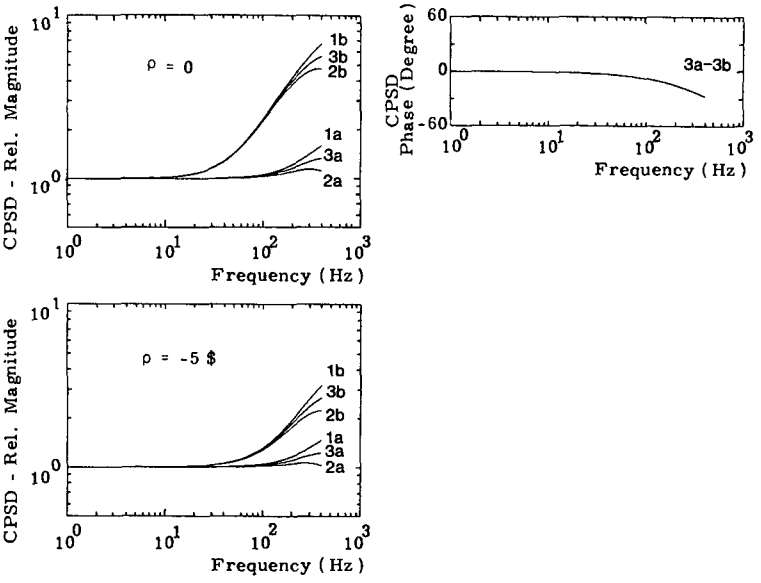

Fig. 10. Relative CPSDs of excore detectors in the critical state and in a subcritical state at −5 $. Curve 1: detector position $x_1 = x_2$ = reflector peak; curve 2: detector position $x_1 = x_2$ = reflector peak + 20 cm; curve 3: detector position x_1 = reflector peak, x_2 = reflector peak + 20 cm. Index (a), $H = 77.6$ cm; index (b), $H = 197$ cm.

of ξ was found to be insensitive to variations of detector position in the vicinity of the thermal flux peak—e.g. the difference in the curves of ξ, when both detectors are located directly at the core–reflector interface or both detectors are located at the position of the thermal flux peak or even one or two diffusion lengths further apart, is so small, that it cannot be fully resolved in the graphical representation. Phase relations in the $CPSD_R$ for separated detectors are independent of the core size and reactivity. A case is included in Fig. 10 (curve 2) in which both detectors are placed a little deeper in the reflector. There is an indication that ξ will pass through a maximum and then decrease. It seems that the reflector behaves as a low-pass filter cutting-off higher-frequency components as more material is introduced between the points of observation and the core boundary.

The coherence function for separate detector positions (within the spatial region investigated) was found to be almost 1 throughout the frequency range considered and was independent of the core size and reactivity. We feel, that this feature may be attributed to the 1-D character of the model.

In Fig. 10, the curves 1a are of most interest. The increase of ξ with frequency, starting at about 100 Hz, is in agreement with the experimental results shown in Figs 3 and 4 (second curve from the top). There is also fairly good agreement in the magnitude although this may be fortuitous. The spatial effects appearing in the measurements are somewhat larger than predicted by the model calculation.

In order to check the validity of our numerical results which are based on two-group diffusion theory, Amato (1981) recently calculated the kinetic importance functions and the $CPSD_R$s for the critical realistic system using the 1-D transport code TASK in two groups and the $S-2$ approximation. The infinite reflector was replaced by a finite reflector of 30 cm length. The $CPSD_R$s (magnitude and phase) and coherence functions were found to be in good agreement with our calculations for the various incore, excore and incore/excore detector locations. The differences in the values of the magnitude of the $CPSD_R$s between our two-group diffusion theory calculations and the ones obtained by using the aforementioned transport code were within 2% at 100 Hz and 8% at 400 Hz.

6.4. *Application to the zero-crossing correlation method*

The cross-correlation function (CCF) is obtained by applying the inverse Fourier transform to the $CPSD_R$. We will relate the CCF to current signal fluctuations including signal conditioning rather than to count-rates. For both detectors located at the same position, the CCF is a symmetrical function with respect to the time lag τ, and follows from

$$\mathrm{CCF}(\mathbf{x}_1 = \mathbf{x}_2, \tau) = \frac{\bar{q}^2}{2\pi}\int_0^\infty \mathrm{d}\omega\xi(\mathbf{x}_1 = \mathbf{x}_2, \omega)\mathrm{PSD}_P(\omega)|H(\omega)|^2\cos\omega\tau. \quad (37)$$

Equation (37) has been written so that ξ appears as a spatial correction term to the point-kinetics results. $H(\omega)$ is the transfer function of the band-pass filter in each channel, consisting of a single RC high-pass filter and a double RC low-pass filter. q is the charge released per detected neutron (both detectors assumed to have identical operational characteristics).

According to the previous spectra investigations, the appearance of space effects in the CCF depends on the frequency region where ξ begins to increase from 1, and also on the reactivity. If this frequency region is sufficiently far above α_c, space-dependent contributions to the CCF are expected to be small in very slightly subcritical states, in spite of the fact that the magnitude of ξ shows a greater variation in these states than in more subcritical states. When, with increasing subcriticality, the plateau and the roll-off of the PSD_P extend to higher frequencies, space-dependent contributions can become appreciable. They can be reduced to some extent by a proper setting of the high-frequency cut-off in the filter function.

Figure 11 shows the results of the calculated reactivity-dependence of the zero-crossing point of the CCF obtained using data of the filter function as used in the experimental setup. Curve 1 refers to the space-independent case with $\xi = 1$ for all frequencies, curve 2 to the favourable case with both detectors located in the middle of the core, where according to Fig. 5 the space effects are very small, and curve 3 to the case where both detectors are located in the reflector zone at the position of the thermal-flux peak. It can be seen that in the realistic system (upper part of Fig. 11) the point-kinetics approximation holds very well, even for the excore detector locations. In the large system (lower part of Fig. 11), measurements with both detectors at the core centre would also follow the point-kinetics approximation fairly well, while measurements with excore detectors would exhibit a significant difference, since the spatial effects begin at frequencies as low as α_c. Curves for other coincident incore detector positions at a distance away from the core centre in the direction of the free core boundary (but not too near the edge) should range between the two space-dependent cases shown in Fig. 11. This is expected from the similar shapes of the relative $CPSD_R$s in Figs 5 and 10, and the comparable order of magnitude of the space effects involved in these curves.

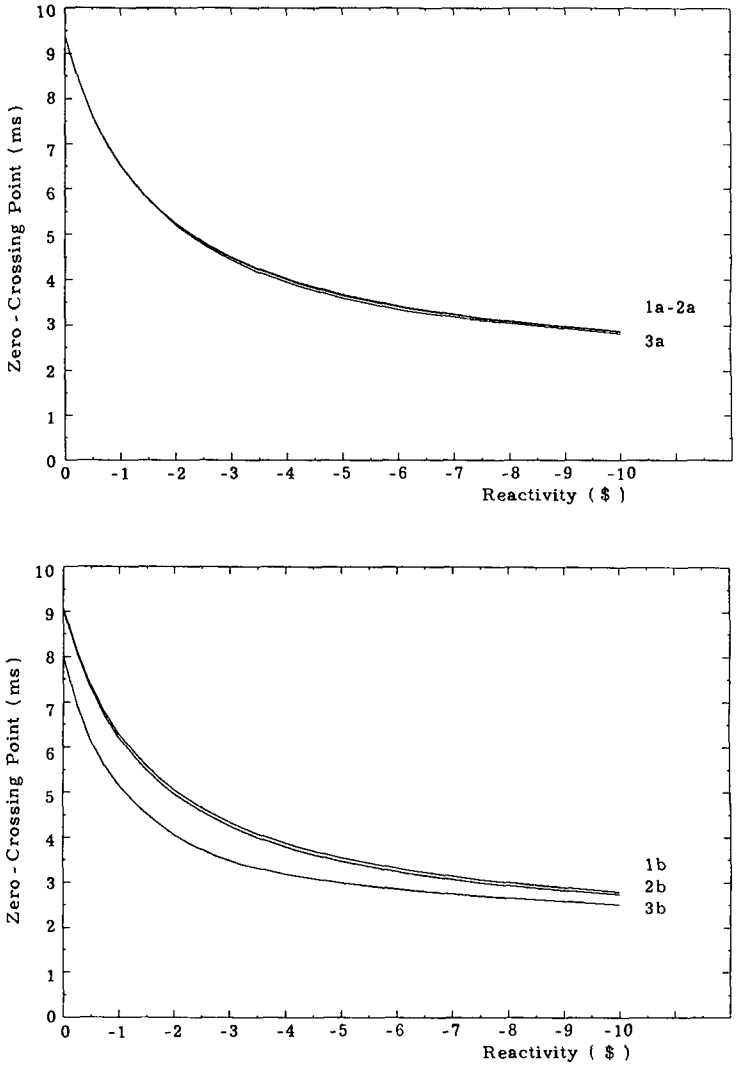

Fig. 11. Zero-crossing point of the cross-correlation function vs reactivity with band-pass filtered detector signals (single RC low-frequency cutoff at 15 Hz, double RC high-frequency cutoff at 200 Hz). Curve 1: point model; curve 2: detector position $\mathbf{x}_1 = \mathbf{x}_2 = 0.5 \times H$; curve 3: detector position $\mathbf{x}_1 = \mathbf{x}_2$ = reflector peak. Index (a) (upper figure), $H = 77.6$ cm; Index (b) (lower figure), $H = 197$ cm.

The zero-crossing point of the CCF was obtained from graphical plots. For the space-independent case and in the prompt-neutron approximation, the CCF can easily be represented by an analytical expression. The inclusion of space effects required a numerical treatment of equation (37) and this was achieved by applying the finite inverse Fourier transform to the CPSD_R via an FFT-algorithm. The integration limits in frequency were successively extended below and above the filter band-pass until convergence was achieved for a given accuracy of the result.

6.5. *Distributed detectors*

If each detector is uniformly distributed over a certain region of the reactor system, the count-rate cross-power spectral density CPSD_{RD} referring to the volumes V_1, V_2 occupied by the detectors, is given by

$$\mathrm{CPSD}_{RD}(V_1,V_2,\omega) = \int_{V_1}\int_{V_2} \mathrm{d}V_1\, \mathrm{d}V_2 \mathrm{CPSD}_R(\mathbf{x}_1,\mathbf{x}_2,\omega). \tag{38}$$

Distributed detectors are certainly unrealistic, because they can never be realized in practice. It is of interest to

consider them for cases when the occupied volumes correspond to system zones. Equation (38) should then yield results which should approach the simple treatment of the reflected system by using a two-point model and two energy groups, except that the core size does not enter as a fixed parameter.

Four cases of distributed detectors were considered:

—both detectors distributed over the core region;
—one detector distributed over the core region, the other one distributed over the reflector region;
—both detectors distributed over the reflector region;
—both detectors distributed throughout the complete system.

The results are shown in Fig. 12. The relative $CPSD_{RD}$ of overlapping incore detectors (curves 2, 6) is close to unity in the frequency range considered. There seems to be a discrepancy between the present results and those given by the one-group two-node treatment of Cohn (1962), according to which there should be an increase of ξ above α when this $CPSD_{RD}$ of the reflected system is compared to the PSD_P of the equivalent bare reactor. Analytis (1981) checked the numerical example given by Cohn. Cohn used an extremely high value for the neutron lifetime in the reflector in his model calculation. The discrepancy vanishes, if a lower, more realistic value is inserted. In addition, Cohn's approach uses separate lifetimes for the core and the reflector while our comparison is based on a PSD_P with a weighted overall generation time including the reflector. Cohn (1964) stated in a later note, that in reflected-reactor kinetics, when the lifetimes do not differ by large orders of magnitude, the combined core and reflector could be treated reasonably well as a single-region system with an equivalent lifetime. Thus we feel that the behaviour of the relative $CPSD_{RD}$ of the incore detectors and the very similar behaviour of the relative $CPSD_{RD}$ of detectors distributed through the complete system (curves 3, 7 in Fig. 12) indicate the validity of this approach.

The relative $CPSD_{RD}$ (magnitude and phase) and the coherence function of a distributed incore detector and

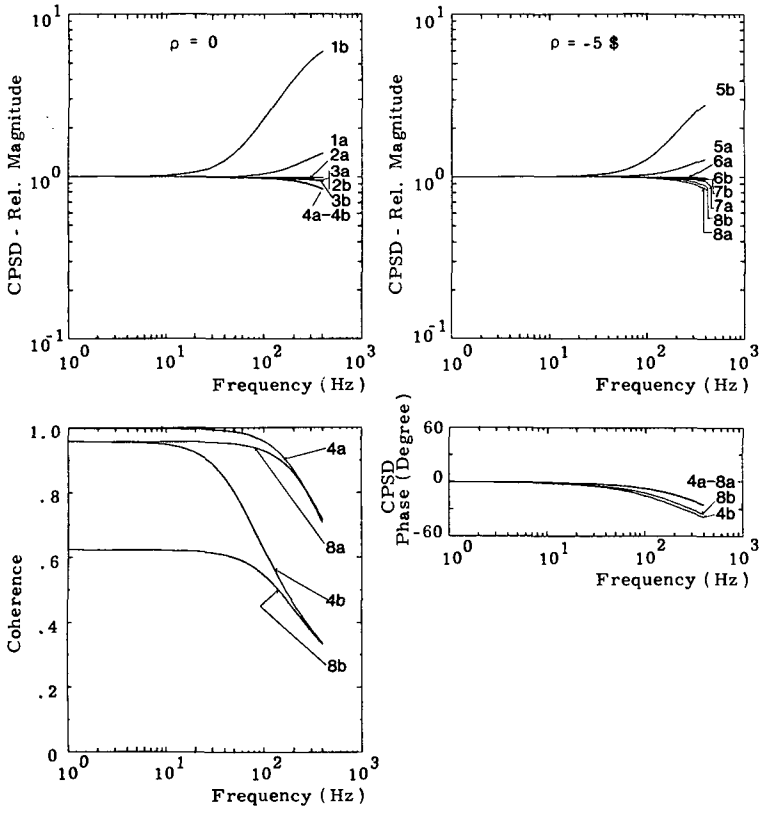

Fig. 12. Relative CPSDs and coherence functions of distributed detectors. Curves 1, 5: detector position $x_1 = x_2$ = reflector zone; curves 2, 6: detector position $x_1 = x_2$ = core zone; curves 3, 7: detector position $x_1 = x_2$ = core + reflector zones; curves 4, 8: detector position x_1 = core zone, x_2 = reflector zone. Curves 1–4: critical state; curves 5–8: subcritical state at −5 $; Index (a), H = 77.6 cm; index (b), H = 197 cm.

a distributed excore detector (curves 4, 8) show an obvious weighted behaviour when compared to the point-detector cases. The relative $CPSD_{RD}$ for both detectors distributed over the reflector (curves 1, 5) exhibits a behaviour similar to that of the relative $CPSD_R$ for point detectors when they are located in the reflector near the core boundary (see Fig. 10). This is not surprising since for distributed detectors only the reflector region near the core gives a significant contribution to the noise. One may conclude, that (within the frame of our 1-D model) the actual size of a practical detector located in the reflector zone does not have an important influence on the spectral shape of the $CPSD_R$.

7. CONCLUSIONS

The work reported is part of a programme to investigate a neutron-noise method in the time domain, i.e. the zero-crossing correlation method, for measuring prompt-neutron decay constants and small negative reactivities, and its practical applicability on a swimming-pool research power reactor. There is a restriction in the measurement, i.e. the neutron detectors can be positioned only in the reflector zone near the core–reflector interface. This constraint immediately raises the question of the extent to which space–energy effects might invalidate the applicability of the point-kinetics approach to the analysis.

As far as we could check the literature, the problem of space effects in neutron-noise analysis in a reflected system has not been extensively investigated. There are only a few examples of measurements with excore detectors. These measurements have been performed on 'clean' facilities and did not give a clear indication of the extent to which space effects are present.

Our investigations have been divided into two parts: experimental and theoretical.

The experimental investigations yield the following results:

—There is no problem in achieving a sufficiently high detection efficiency with detectors located in the reflector zone near the core and to measure the neutron correlations with a high accuracy within a reasonable measuring time. The detection efficiency may be influenced by the γ-background which becomes important in subcritical states. This possible influence is, however, of minor importance. An indication of other disturbing effects from the γ-background was not found in the data analysis.

—Measurements of cross-power spectra show an increasing deviation from point kinetics at higher frequencies starting at about 100 Hz. The roll-off of the cross-spectra becomes weaker than predicted by the point-kinetics reactivity transfer function. This behaviour indicates the presence of space–energy effects. The zero-crossing correlation method analyses the reactivity-dependent break characteristics. For subcritical states below -5 \$, the method becomes insensitive. The reactivity transfer function acts itself as a low-pass filter cutting-off higher-frequency components. For slightly subcritical states, the values of the break frequency α are much below the frequency region where the space effects appear. In more subcritical states, when the plateau in the reactivity transfer function extends to higher frequencies, the low-pass filter in the signal conditioner which confines the detection–noise component helps to reduce the influence of spatial effects.

—The use of the point-kinetics model in the data analysis is a very good approximation. α-values obtained from the zero-crossing correlation method and from simultaneously-measured cross-spectra, evaluated below 100–150 Hz, were in good agreement. Reactivity determinations were also found to agree with results obtained by the rod-drop method. Varied detector positions around the core with different detector separations did not show any observable space effect in the α_c- and reactivity-determination (except for the obvious effect that a change of detector positions can be accompanied by a change in the reactivity worth of the chambers).

Most of this work is concerned with a theoretical investigation of the space–energy effects to be expected in neutron-noise analysis in a reflected LWR. The investigation has been performed on a simple 1-D model consisting of a homogeneous core and a one-sided infinite homogeneous reflector using two-group diffusion theory and the Langevin technique with a noise-equivalent source of the fission process. In order to obtain a deeper insight, the calculations have not been confined to detector locations in the reflector zone, but have been extended to other detector locations (both detectors incore or one detector incore and one in the reflector). The detectors are assumed to be sensitive to thermal neutrons only. Fast fission has been neglected. Its inclusion in the numerical treatment would mainly increase the computer time without significantly altering the picture of the space effects appearing in the cross-spectra.

The important results of the theoretical investigation can be summarized as follows:

—The model reproduces the shape of the cross-spectra found in the experiments when both detectors are located in the reflector zone near the core boundary. Using data thought to be realistic, the frequency

region where space effects appear and also the magnitude of the space effects appearing in the spectra are of the same order when compared with the experimental findings. Applying the model calculation to the zero-crossing correlation method with the same instrumental data as used in the measurements reveals that the point-kinetics approximation holds very well. In spite of the fact that space-dependent noise theories have had little verification, we believe that our theoretical results strongly support the applicability of the point-kinetics approximation.

—The space-dependent characteristics of the cross-spectra and coherence functions for incore detectors are not typical of the reflected system. They are influenced by the reflector, but not very strongly. A light-water reflector is in principle a bad reflector. Very similar characteristics can also be obtained for the bare reactor. With increasing frequency, the coupling of the neutron field decreases. Increasing core size shifts the onset of the decoupling to lower frequencies and finally, for widely-spaced detectors, leads to the appearance of a sink structure in the cross-spectra at higher frequencies. This sink structure is well known in coupled-core kinetics. The same behaviour is also manifested in the cross-spectra when one detector is excore. The breakdown of point kinetics in such cases is not a new result, but rather a confirmation of the validity of our calculations.

It must be emphasized that the statements made in this paper refer to a light-water-moderated reactor with a light-water reflector. For highly-reflected systems, space-dependent effects start becoming important at frequencies as low as those associated with the delayed neutrons.

In the introduction of statistical methods to assist reactor-operation problems of a swimming-pool reactor, the reactivity meter can be regarded as a useful item of equipment. Its special feature is that it allows a rapid measurement of α_c. The knowledge of α_c is not necessary for the operation of a reactor, but is required in safety evaluations of dynamic transients.

Acknowledgements—The first coauthor is indebted to the International Atomic Energy Agency (IAEA) for a one-year fellowship allowing a stay at EIR, and to Professor H. Gränicher, director of EIR, who made it possible to continue the work by means of a Swiss fellowship.

Experiments on a reactor always need the assistance of many people. Thanks are due to the operational staff of SAPHIR and particularly its leader, Mr H. Winkler. Mr J. Phildius helped in the measurements. We are indebted to Mr B. Leoni who designed the detector setup and had to solve several initial troubles. Thanks are due to Dr R. Richmond who read the manuscript and improved our English.

REFERENCES

Ackermann N. J., Penland J. R. and Hanauer S. H. (1971) *Trans Am. nucl. Soc.* **14,** 854.
Albrecht R. W. and Danofsky R. A. (1969) *Trans Am. nucl. Soc.* **12,** 708.
Albrecht R. W. and Seifritz W. (1968) *Nukleonik* **11,** 143.
Amato H. G. (1981) Private communication.
Analytis G. Th. (1981) Private communication.
Analytis G. Th. (1982) *Ann. nucl. Energy* **9,** 53.
Behringer K. and Peier W. (1979) *Nucl. Instrum. Meth.* **161,** 97.
Behringer K. and Phildius J. (1974) *Nucl. Instrum. Meth.* **116,** 45.
Behringer K., Jeschki W., Pruys H. S. and Seifritz W. (1974a) *Reaktortagung des Deutschen Atomforums/KTG*, Berlin, 2–5 April.
Behringer K., Jeschki W., Leoni B., Phildius J., Pruys H. S. and Seifritz W. (1974b) *Trans Am. nucl. Soc.* **18,** 302.
Behringer K., Phildius J. and Seifritz W. (1975) *Ann. nucl. Energy* **2,** 399.
Behringer K., Kosály G. and Kostić Lj. (1977) *Nucl. Sci. Engng* **63,** 306.
Behringer K., Kosály G. and Pázsit I. (1979) *Nucl. Sci. Engng* **72,** 304.
Bendat J. S. and Piersol A. G. (1971) *Random Data: Analysis and Measurement Procedures.* Wiley-Interscience, New York.
Buhl A. R., Hanauer S. H. and Baumann N. P. (1968) *Nucl. Sci. Engng* **34,** 98.
Cohn Ch. E. (1959) *Nucl. Sci. Engng* **6,** 284.
Cohn Ch. E. (1960) *Nucl Sci. Engng* **7,** 472.
Cohn Ch. E. (1962) *Nucl. Sci. Engng* **13,** 12.
Cohn Ch. E. (1964) *Noise Analysis in Nuclear Systems* (Ed. Uhrig R. E.), p. 307. USAEC.
Dam H. van (1976) *Atomkernenergie* **27,** 8.
Dam H. van (1977) *Ann. nucl. Energy* **4,** 185.
Demarmels P. (1968) *IAEA Panel on Reactivity Measurements*, Vienna, 9–13 December.
Dragt J. B. (1966) *Nukleonik* **8,** 188.
Ebert D. D., Clement J. D. and Stacey W. M. (1974a) *Nucl. Sci. Engng* **55,** 368.
Ebert D. D., Clement J. D. and Stacey W. M. (1974b) *Nucl. Sci. Engng* **55,** 380.
Genoud J. P. (1977) *Ann. nucl. Energy* **4,** 435.
Gozani T. (1963) *Nukleonik* **5,** 55.
Hendrickson R. A. and Danofsky R. A. (1967) *Measurement of the Reactivity Coupling Coefficient in the Iowa State UTR-10*, p. 506. Texas A & M Univ. Press.
Koehler P. (1980) Private communication.
Kosály G., Meskó L. and Pázsit I. (1977) *Ann. nucl. Energy* **4,** 79.
Lescano V. H. and Behringer K. (1981) EIR-Report 446.
Meem J. L. (1964) *Two Group Reactor Theory.* Gordon & Breach, New York.
Morishima N. (1979) *Ann. nucl. Energy* **6,** 553.
Nagy M. E., Sawan M. E. and Shaat M. K. (1979) *Atomkernenergie* **34,** 261.
Natelson M., Osborn R. K. and Shure F. (1966) *J. nucl. Energy* **20,** 557.
Nieto J. M., Akhtar P. and Ackermann N. J. (1968) *J. nucl. Energy* **22,** 675.
Otsuka M. and Iijima T. (1965) *Nukleonik* **7,** 488.
Pázsit I. (1978) *Ann. nucl. Energy* **5,** 185.
Penland J. R. and Hanauer S. H. (1968) *Trans Am. nucl. Soc.* **11,** 563.

Penland J. R., Ackermann N. J. and Hanauer S. H. (1971) *Trans. Am. nucl. Soc.* **14,** 854.
Preskitt C. A., Nephew E. A., Brown J. R. and Van Howe K. R. (1967) *Nucl. Sci. Engng* **29,** 283.
Randall R. L. and Griffin C. W. (1964) *Noise Analysis in Nuclear Systems* (Ed. Uhrig R. E.), p. 107. USAEC.
Ricker C. W., Hanauer S. H. and Mann E. R. (1968) *Nucl. Sci. Engng* **33,** 56.
Robinson J. C. and Alexander M. L. (1971) *Trans Am. nucl. Soc.* **14,** 856.
Saito K. (1967a) *Nucl. Sci. Engng* **28,** 384.
Saito K. (1967b) *Nucl. Sci. Engng* **28,** 452.
Saito K. (1979) *Prog. nucl. Energy* **3,** 157.
Seifritz W. and Albrecht R. W. (1968) *Nukleonik* **11,** 149.
Seifritz W. and Stegemann D. (1971) *Atom. Energy Rev.* **9,** 129.
Sheff J. R. (1968) *Trans Am. nucl. Soc.* **11,** 233.
Sheff J. R. (1969) *Trans Am. nucl. Soc.* **12,** 709.
Sheff J. R. and Albrecht R. W. (1966a) *Nucl. Sci. Engng* **24,** 246.
Sheff J. R. and Albrecht R. W. (1966b) *Nucl. Sci. Engng* **26,** 207.
Süssmann H. F., Brixy H. and Hecker R. (1976) Jül-Report 1368.
Thomas C. O., Hanauer S. H. and Baumann N. P. (1973) *Nucl. Sci. Engng* **51,** 253.
Viehl E. (1975) *Nucl. Sci. Engng* **56,** 422.
Williams M. M. R. (1966) *J. nucl. Energy* **21,** 321.
Williams M. M. R. (1974) *Random Processes in Nuclear Reactors.* Pergamon Press, Oxford.
Winkler H. and Koehler P. (1975) Internal EIR-Report.

APPENDIX A

Static Flux Shapes

The static flux calculation in two energy groups for a symmetrical slab reactor system consisting of a homogeneous core with a homogeneous reflector on both sides can be found in any standard work on reactor theory. The modifications necessary for our asymmetrical model are minor. For completeness, a brief review will be given.

The multiplication eigenfunctions $\varphi_1(\mathbf{x})$, $\varphi_2(\mathbf{x})$ in the fast and thermal groups, respectively, are given by the equations in the core zone $0 \leqslant \mathbf{x} \leqslant H$:

$$\begin{pmatrix} D_1 \dfrac{\mathrm{d}^2}{\mathrm{d}\mathbf{x}^2} - \Sigma_1, & \dfrac{\nu\Sigma_f}{k} \\ \Sigma_R, & D_2 \dfrac{\mathrm{d}^2}{\mathrm{d}\mathbf{x}^2} - \Sigma_2 \end{pmatrix} \begin{pmatrix} \varphi_1 \\ \varphi_2 \end{pmatrix} = 0 \tag{A.1}$$

and in the reflector zone $\mathbf{x} \geqslant H$, where for distinction all quantities are denoted by an index R:

$$\begin{pmatrix} D_{1R} \dfrac{\mathrm{d}^2}{\mathrm{d}\mathbf{x}^2} - \Sigma_{1R}, & 0 \\ \Sigma_{RR}, & D_{2R} \dfrac{\mathrm{d}^2}{\mathrm{d}\mathbf{x}^2} - \Sigma_{2R} \end{pmatrix} \begin{pmatrix} \varphi_{1R} \\ \varphi_{2R} \end{pmatrix} = 0. \tag{A.2}$$

According to the assumption made for the extraneous source in the core region, that its spatial distribution follows the shape of the critical thermal flux, the static subcritical fluxes ϕ_1, ϕ_2 correspond to the solution of the eigenfunctions φ_1, φ_2 for the largest eigenvalue $k = k_1$.

The solution of φ_1, φ_2 in the core zone, which satisfies to the boundary condition of vanishing at $\mathbf{x} = 0$, takes the form:

$$\varphi_1(\mathbf{x}) = a \sin \mu\mathbf{x} + c \sinh \lambda\mathbf{x} \tag{A.3a}$$

$$\varphi_2(\mathbf{x}) = aS_\mu \sin \mu\mathbf{x} + cS_\lambda \sinh \lambda\mathbf{x} \qquad 0 \leqslant \mathbf{x} \leqslant H, \tag{A.3b}$$

where:

principal buckling,

$$\mu^2 = -\frac{1}{2}\frac{\tau + L^2}{\tau L^2}\left\{1 - \sqrt{\left[1 + \frac{4\tau L^2}{(\tau + L^2)^2}\left(\frac{k_\infty k_1}{k_n} - 1\right)\right]}\right\} \tag{A.4a}$$

alternate buckling,

$$\lambda^2 = \frac{1}{2}\frac{\tau + L^2}{\tau L^2}\left\{1 + \sqrt{\left[1 + \frac{4\tau L^2}{(\tau + L^2)^2}\left(\frac{k_\infty k_1}{k_n} - 1\right)\right]}\right\} \tag{A.4b}$$

infinite multiplication factor,

$$k_\infty = \frac{\nu\Sigma_f\Sigma_R}{k_1\Sigma_1\Sigma_2} \tag{A.4c}$$

Fermi age,

$$\tau = \frac{D_1}{\Sigma_1} \tag{A.4d}$$

thermal diffusion area,

$$L^2 = \frac{D_2}{\Sigma_2} \tag{A.4e}$$

principal coupling coefficient,

$$S_\mu = \frac{\Sigma_R}{D_2}\frac{1}{\mu^2 + \dfrac{1}{L^2}} \tag{A.4f}$$

alternate coupling coefficient,

$$S_\lambda = \frac{\Sigma_R}{D_2}\frac{1}{-\lambda^2 + \dfrac{1}{L^2}} = -\frac{\Sigma_R}{D_2}\frac{1}{\mu^2 + \dfrac{1}{\tau}}. \tag{A.4g}$$

For $n = 1$, the bucklings correspond exactly to those of the critical-core fluxes (fundamental mode bucklings).

The solution of the reflector equations (A.2) with the condition of vanishing when $\mathbf{x} \to \infty$, can be expressed by the interface fluxes at $\mathbf{x} = H$:

$$\varphi_{1R}(\mathbf{x}) = \exp[\gamma(\mathbf{x} - H)]\varphi_{1R}(H) \tag{A.5a}$$

$$\varphi_{2R}(\mathbf{x}) = S_R\{\exp[\delta(\mathbf{x} - H)] - \exp[\gamma(\mathbf{x} - H)]\} \times \varphi_{1R}(H) + \exp[\delta(\mathbf{x} - H)]\varphi_{2R}(H) \qquad \mathbf{x} \geqslant H, \tag{A.5b}$$

where:

reflector Fermi age,

$$\tau_R = \frac{D_{1R}}{\Sigma_{1R}} \tag{A.6a}$$

reflector thermal diffusion area,

$$L_R^2 = \frac{D_{2R}}{\Sigma_{2R}} \tag{A.6b}$$

reflector coupling coefficient,

$$S_R = \frac{\Sigma_{RR}}{D_{2R}} \frac{\tau_R L_R^2}{\tau_R - L_R^2} = \frac{\Sigma_{RR}}{\Sigma_{2R}} \frac{\tau_R}{\tau_R - L_R^2} \tag{A.6c}$$

and

$$\gamma = -\frac{1}{\sqrt{\tau_R}} \tag{A.6d}$$

$$\delta = -\frac{1}{L_R}. \tag{A.6e}$$

The normal continuity requirements of the fluxes and currents across the interface between the two zones,

$$\varphi_1(H) = \varphi_{1R}(H) \tag{A.7a}$$

$$\varphi_2(H) = \varphi_{2R}(H) \tag{A.7b}$$

$$D_1\left(\frac{d\varphi_1}{dx}\right)_H = D_{1R}\left(\frac{d\varphi_{1R}}{dx}\right)_H \tag{A.8a}$$

$$D_2\left(\frac{d\varphi_2}{dx}\right)_H = D_{2R}\left(\frac{d\varphi_{2R}}{dx}\right)_H, \tag{A.8b}$$

lead to the equation for the eigenvalues k_n, which can be expressed according to Meem (1964) by

$$p = \frac{r_2\delta C_1 + r_1\gamma C_2 + qC_3}{C_1 + C_2 + C_3}, \tag{A.9}$$

with the following abbreviations:

$$p = \left(\frac{1}{\varphi_1}\frac{d\varphi_1}{dx}\right)_{H,c=0} = \mu \operatorname{ctg} \mu H \tag{A.10a}$$

$$q = \left(\frac{1}{\varphi_1}\frac{d\varphi_1}{dx}\right)_{H,a=0} = \lambda \operatorname{ctgh} \lambda H \tag{A.10b}$$

$$r_1 = D_{1R}/D_1 \tag{A.10c}$$

$$r_2 = D_{2R}/D_2 \tag{A.10d}$$

$$C_1 = S_\mu(r_1\gamma - q) \tag{A.10e}$$

$$C_2 = S_2(q - r_2\delta) \tag{A.10f}$$

$$C_3 = r_2 S_R(\delta - \gamma). \tag{A.10g}$$

For the critical system ($k_1 = 1$), the equation (A.9) connects the group parameters with the critical dimension H. It represents an equivalent relation to that of equalizing material buckling and geometrical buckling as at a bare homogeneous reactor. Unfortunately, it is a highly transcendental equation and cannot be solved analytically for H, or if H is given, for the eigenvalues k_n.*

When equation (A.9) is solved, one can then establish a relation between a and c in equation (A.3a) using equations (A.7a), (A.8a) and (A.5a)

$$a(p - r_1\gamma)\sin \mu H + c(q - r_1\gamma)\sinh \lambda H = 0. \tag{A.11}$$

If one sets

$$a = \frac{q - r_1\gamma}{\sin \mu H} a_0 \tag{A.12a}$$

$$c = -\frac{p - r_1\gamma}{\sinh \lambda H} a_0, \tag{A.12b}$$

* In our case, only k_1 is needed.

where a_0 can be related, for example, to the extraneous source strength, the fluxes can finally be written as:

$$\varphi_1(x) = a_0\left(\frac{q - r_1\gamma}{\sin \mu H}\sin \mu x - \frac{p - r_1\gamma}{\sinh \lambda H}\sinh \lambda x\right) \tag{A.13a}$$

$$0 \leqslant x \leqslant H$$

$$\varphi_2(x) = a_0\left(S_\mu\frac{q - r_1\gamma}{\sin \mu H}\sin \mu x - S_\lambda\frac{p - r_1\gamma}{\sinh \lambda H}\sinh \lambda x\right) \tag{A.13b}$$

and

$$\varphi_{1R}(x) = a_0(q - p)\exp[\gamma(x - H)] \tag{A.14a}$$

$$x \geqslant H$$

$$\varphi_{2R}(x) = [\![a_0 S_R(q - p)\{\exp[\gamma(x - H)] - \exp[\delta(x - H)]\} + [S_\mu q - S_\lambda p - r_1\gamma(S_\mu - S_\lambda)]\exp[\delta(x - H)]]\!]. \tag{A.14b}$$

APPENDIX B

Kinetic Importance Functions

The functional dependence of the kinetic importance functions on space, detector location and frequency in our reflected-reactor model can be represented by a closed analytical solution. The solution procedure is very similar to the static flux calculation. We have to distinguish the two cases: detector in the core and detector in the reflector.

We consider first the case when the detector is located in the reflector at a space point $x_1 > H$. According to the general definition of the kinetic importance functions by equations (8), the system of equations to be solved is:

For the core $0 \leqslant x \leqslant H$

$$\begin{pmatrix} D_1\frac{d^2}{dx^2} - \Sigma_1', & \Sigma_R \\ \nu\Sigma_f(1-h), & D_2\frac{d^2}{dx^2} - \Sigma_2' \end{pmatrix}\begin{pmatrix}\phi_1^+ \\ \phi_2^+\end{pmatrix} = 0 \tag{B.1}$$

and for the reflector $x \geqslant H$

$$\begin{pmatrix} D_{1R}\frac{d^2}{dx^2} - \Sigma_{1R}', & \Sigma_{RR} \\ 0, & D_{2R}\frac{d^2}{dx^2} - \Sigma_{2R}' \end{pmatrix}\begin{pmatrix}\phi_{1R}^+ \\ \phi_{2R}^+\end{pmatrix} = -\delta(x - x_1)\begin{pmatrix}\Sigma_{1d} \\ \Sigma_{2d}\end{pmatrix}. \tag{B.2}$$

The solution in the core zone satisfying the boundary condition at $x = 0$ can be written as

$$\phi_1^+ = \mathbb{A}^+ \sin \mu' x + \mathbb{C}^+ \sinh \lambda' x \tag{B.3a}$$

$$0 \leqslant x \leqslant H$$

$$\phi_2^+ = \mathbb{A}^+ S_\mu^+ \sin \mu' x + \mathbb{C}^+ S_\lambda^+ \sinh \lambda' x \tag{B.3b}$$

$\mathbb{A}^+$ and $\mathbb{C}^+$ are complex functions of the frequency and the space point x_1 of the detector location in the reflector zone. The bucklings are frequency-dependent quantities, given by

$$\mu'^2 = -\frac{1}{2}\frac{\tau' + L^2}{\tau' L^2} \times \left\{1 - \sqrt{\left[1 + \frac{4\tau' L^2}{(\tau' + L^2)^2}\left(\frac{k_\infty k(1-h)\tau' L^2}{\tau L^2} - 1\right)\right]}\right\} \tag{B.4a}$$

$$\lambda'^2 = \frac{1}{2}\frac{\tau'+L'^2}{\tau' L'^2} \times \left\{1+\sqrt{\left[1+\frac{4\tau' L'^2}{(\tau'+L'^2)^2}\left(\frac{k_\infty k(1-h)\tau' L'^2}{\tau L'^2}-1\right)\right]}\right\}, \tag{B.4b}$$

where τ' and L'^2 denote a frequency-dependent Fermi age and a frequency-dependent thermal diffusion area, respectively, defined by $\tau' = D_1/\Sigma_1'$ and $L'^2 = D_2/\Sigma_2'$. S_μ^+ and S_λ^+ can be called adjoint coupling coefficients and are also complex functions of the frequency.

$$S_\mu^+ = \frac{\nu\Sigma_f(1-h)}{D_2\left(\mu'^2+\frac{1}{L'^2}\right)} = \frac{D_1}{\Sigma_R}\left(\mu'^2+\frac{1}{\tau'}\right) \tag{B.5a}$$

$$S_\lambda^+ = \frac{\nu\Sigma_f(1-h)}{D_2\left(-\lambda'^2+\frac{1}{L'^2}\right)} = \frac{D_1}{\Sigma_R}\left(-\lambda'^2+\frac{1}{\tau'}\right). \tag{B.5b}$$

For frequencies that are not too high, and for slightly-subcritical states, the μ-root of equation (B.4a) contains in particular the infinite-core reactivity transfer function. Or one can use a more realistic approach by introducing the bare-core equivalent reactivity transfer function through a fictitious geometrical buckling satisfying the criticality equation (see also Appendix C). Due to the reflector saving an equivalent bare reactor is larger in size than the core of the reflected reactor. In both concepts, however, the overall kinetics are finally determined by the coupling with the reflector properties. A core volume distributed source will make a dominant contribution from almost all core points to the detector response via the corresponding μ-term in the equations (B.3a,b). In the higher frequency range when the reactivity transfer function is dying out and higher prompt modes implicitly appear, the μ-term contribution can compete with the λ-term contribution in equation (B.3a,b). The λ-root of equation (B.4b) represents a typical spectrum effect and is not present in a one-group treatment. It can be approximated by $\lambda' \sim 1/L$, since τ is $\gg L^2$ in LWRs. It becomes appreciably frequency dependent in the high-frequency range ($\gtrsim 100$ Hz). The corresponding λ-term shows short spatial-range characteristics. A core volume distributed source contributes to the detector response via this component preferably from a small core region at H only—or in the case of an incore detector, from a small localized field around the detector position.

The solution in the reflector zone with the condition of vanishing for $\mathbf{x} \to \infty$ can most elegantly be obtained by applying the Fourier transform to equation (B.2) with regard to the space variable $\mathbf{x}$. Using the same notation as in Appendix A, but with frequency-dependent reflector Fermi age and reflector thermal diffusion area, the result can be written in a general way without distinguishing the regions $H \leqslant \mathbf{x} < \mathbf{x}_1$ and $\mathbf{x} \geqslant \mathbf{x}_1$.

$$\begin{aligned}\phi_{1R}^+ = {} & \phi_{1R}^+(H)\exp[\gamma'(\mathbf{x}-H] - S_R^+\phi_{2R}^+(H)\{\exp[\delta'(\mathbf{x}-H)] - \exp[\gamma'(\mathbf{x}-H)]\} \\ & + \frac{\Sigma_{1d}}{2D_{1R}}\sqrt{\tau_R'}\{\exp[\gamma'|(\mathbf{x}-H)-(\mathbf{x}_1-H)|] - \exp[\gamma'((\mathbf{x}-H)+(\mathbf{x}_1-H))]\} \\ & + S_R^+\frac{\Sigma_{2d}}{2D_{2R}}[\![\sqrt{\tau_R'}\{\exp[\gamma'|(\mathbf{x}-H)-(\mathbf{x}_1-H)|] - \exp[\gamma'((\mathbf{x}-H)+(\mathbf{x}_1-H))]\} \\ & - L_R'\{\exp[\delta'|(\mathbf{x}-H)-(\mathbf{x}_1 H)|] - \exp[\delta'((\mathbf{x}-H)+(\mathbf{x}_1-H))]\}]\!] \qquad x \geqslant H\end{aligned} \tag{B.6a}$$

$$\phi_{2R}^+ = \phi_{2R}^+(H)\exp[\delta'(\mathbf{x}-H)] + \frac{\Sigma_{2d}}{2D_{2R}}L_R'\{\exp[\delta'|(\mathbf{x}-H)-(\mathbf{x}_1-H)|] - \exp[\delta'((\mathbf{x}-H)+(\mathbf{x}_1-H))]\}, \tag{B.6b}$$

where S_R^+ is the reflector adjoint coupling coefficient

$$S_R^+ = \frac{\Sigma_{RR}}{D_{1R}}\frac{\tau_R' L_R'^2}{\tau_R' - L_R'^2}. \tag{B.7}$$

The spatial relaxation lengths involved in equations (B.6a,b) become appreciably frequency dependent only at high frequencies.

The coefficients $\mathbb{A}^+$ and $\mathbb{C}^+$ in equations (B.3a,b) are obtained by using the interface boundary conditions of equations (A.7) and (A.8). This leads to the following system of equations:

$$\begin{pmatrix} [p'-r_1\gamma'-r_1 S_R^+ S_\mu^+(\gamma'-\delta')]\sinh\mu' H, & [q'-r_1\gamma'-r_1 S_R^+ S_\lambda^+(\gamma'-\delta')]\sinh\lambda' H \\ S_\mu^+(p'-r_2\delta')\sinh\mu' H, & S_\lambda^+(q'-r_2\delta')\sinh\lambda' H \end{pmatrix}\begin{pmatrix}\mathbb{A}^+ \\ \mathbb{C}^+\end{pmatrix} = \begin{pmatrix}F_1 \\ F_2\end{pmatrix}, \tag{B.8}$$

F_1, F_2 in equation (B.8) represent the source functions

$$F_1 = \frac{r_1\Sigma_{1d}}{D_{1R}}\exp[\gamma'(\mathbf{x}_1-H)] + \frac{r_1 S_R^+\Sigma_{2d}}{D_{2R}}\{\exp[\gamma'(\mathbf{x}_1-H)] - \exp[\delta'(\mathbf{x}_1-H)]\} \tag{B.9a}$$

$$F_2 = \frac{r_2\Sigma_{2d}}{D_{2R}}\exp[\delta'(\mathbf{x}_1-H)]. \tag{B.9b}$$

In the second case, when a detector is located in the core zone, $0 < \mathbf{x}_1 < H$, we have to solve the system of equations for the core $0 \leqslant \mathbf{x} \leqslant H$

$$\begin{pmatrix} D_1 \dfrac{\mathrm{d}^2}{\mathrm{d}\mathbf{x}^2} - \Sigma_1', & \Sigma_R \\ \nu\Sigma_f(1-h), & D_2 \dfrac{\mathrm{d}^2}{\mathrm{d}\mathbf{x}^2} - \Sigma_2' \end{pmatrix} \begin{pmatrix} \phi_1^+ \\ \phi_2^+ \end{pmatrix} = -\delta(\mathbf{x}-\mathbf{x}_1) \begin{pmatrix} \Sigma_{1d} \\ \Sigma_{2d} \end{pmatrix} \tag{B.10a}$$

and for the reflector $\mathbf{x} \geqslant H$

$$\begin{pmatrix} D_{1R} \dfrac{\mathrm{d}^2}{\mathrm{d}\mathbf{x}^2} - \Sigma_{1R}', & \Sigma_{RR} \\ 0, & D_{2R} \dfrac{\mathrm{d}^2}{\mathrm{d}\mathbf{x}^2} - \Sigma_{2R}' \end{pmatrix} \begin{pmatrix} \phi_{1R}^+ \\ \phi_{2R}^+ \end{pmatrix} = 0. \tag{B.10b}$$

The solutions can be written as

$$\phi_1^+ = \mathbb{A}^+ \sin \mu'\mathbf{x} + \mathbb{C}^+ \sinh \lambda'\mathbf{x} \tag{B.11a}$$

$$0 \leqslant \mathbf{x} < x_1$$

$$\phi_2^+ = \mathbb{A}^+ S_\mu^+ \sin \mu'\mathbf{x} + \mathbb{C}^+ S_\lambda^+ \sinh \lambda'\mathbf{x} \tag{B.11b}$$

$$\phi_1^+ = \mathbb{A}^+ \sin \mu'\mathbf{x} + \mathbb{C}^+ \sinh \lambda'\mathbf{x} - \mathbb{A}_0^+ \sin \mu'(\mathbf{x}-\mathbf{x}_1) - \mathbb{C}_0^+ \sinh \lambda'(\mathbf{x}-\mathbf{x}_1) \tag{B.11c}$$

$$x_1 \leqslant \mathbf{x} \leqslant H$$

$$\phi_2^+ = \mathbb{A}^+ S_\mu^+ \sin \mu'\mathbf{x} + \mathbb{C}^+ S_\lambda^+ \sinh \lambda'\mathbf{x} - \mathbb{A}_0^+ S_\mu^+ \sin \mu'(\mathbf{x}-\mathbf{x}_1) - \mathbb{C}_0^+ S_\lambda^+ \sinh \lambda'(\mathbf{x}-\mathbf{x}_1) \tag{B.11d}$$

$$\phi_{1R}^+ = \phi_{1R}^+(H)\exp[\gamma'(\mathbf{x}-H)] - S_R^+ \phi_{2R}^+(H)\{\exp[\delta'(\mathbf{x}-H)] - \exp[\gamma'(\mathbf{x}-H)]\} \tag{B.12a}$$

$$\mathbf{x} \geqslant H$$

$$\phi_{2R}^+ = \phi_{2R}^+(H)\exp[\delta'(\mathbf{x}-H)]. \tag{B.12b}$$

Equations (B.12a,b) follow immediately from equations (B.6a,b) by removing the source terms. $\mathbb{A}_0^+$ and $\mathbb{C}_0^+$ in equations (B.11c,d) stand for

$$\mathbb{A}_0^+ = \frac{1}{D_1 D_2(\mu'^2 + \lambda'^2)\mu'} \left(\frac{\nu\Sigma_f(1-h)\Sigma_{1d}}{S_\mu^+} + \Sigma_R \Sigma_{2d} \right) \tag{B.13a}$$

$$\mathbb{C}_0^+ = -\frac{1}{D_1 D_2(\mu'^2 + \lambda'^2)\lambda'} \left(\frac{\nu\Sigma_f(1-h)\Sigma_{1d}}{S_\lambda^+} + \Sigma_R \Sigma_{2d} \right). \tag{B.13b}$$

The coefficients $\mathbb{A}^+$ and $\mathbb{C}+$, which are now dependent on the detector location in the core zone are again determined by equation (B.8), but with the functions F_1, F_2 on the r.h.s.:

$$F_1 = \mathbb{A}_0^+[p_0' - r_1\gamma' - r_1 S_R^+ S_\mu^+(\gamma' - \delta')] \sin \mu'(H-\mathbf{x}_1) - \mathbb{C}_0^+[q_0' - r_1\gamma' - r_1 S_R^+ S_\lambda^+(\gamma' - \delta')] \sinh \lambda'(H-\mathbf{x}_1) \tag{B.14a}$$

$$F_2 = \mathbb{A}_0^+ S_\mu^+[p_0' - r_2\delta'] \sin \mu'(H-\mathbf{x}_1) - \mathbb{C}_0^+ S_\lambda^+[q_0' - r_2\delta'] \sinh \lambda'(H-\mathbf{x}_1), \tag{B.14b}$$

where

$$p_0' = \mu' \operatorname{ctg} \mu'(H-\mathbf{x}_1) \tag{B.15a}$$

$$q_0' = \lambda' \operatorname{ctgh} \lambda'(H-\mathbf{x}_1). \tag{B.15b}$$

The pair of functions F_1, F_2 in equations (B.14a,b) show a steady transition to the other pair of functions in equations (B.9a,b) when the detector is located at the interface with $\mathbf{x}_1 = H$.

One can show, that the determinant on the l.h.s. of equation (B.8) reduces to the criticality equation (A.9) for zero frequency when the reactor is in the critical state, i.e. this determinant becomes zero and the kinetic importance functions diverge for $\omega = 0$. This behaviour reflects the physical fact that a critical reactor is in a labile equilibrium state, if the presence of power and control feedbacks are disregarded. There is no power to drive a critical system into a defined equilibrium position. This leads also to a divergency of the CSPD_R at zero-frequency or likewise to a divergency of the count-rate cross-correlation function* for any delay time. As Dragt (1966) pointed out, the consideration is correct for any system which has a Green's function with a zero-pole, but it is based on the assumption of an infinitely-long measuring time. In practice, however, estimates are always based on a finite measuring time which eliminates this divergency. The zero-crossing correlation method has the further feature, that it avoids this divergency problem by high-pass filtering of the detector signal fluctuations.

The interpretation of the solution of the kinetic importance functions is extremely complicated. Any efforts to try rigorous approximations and to investigate their validity ranges are

* More exactly, it is a covariance function.

more complex than the application of the given formulae by straightforward programming without any approximations.

APPENDIX C

Space-effects in the Count-rate Cross-power

Spectral density in a bare homogeneous reactor

The appearance of spatial effects in the CPSD_R of detectors located in a bare homogeneous reactor depends decisively upon the system dimension H. In this appendix the conditions yielding approximately space-independent results are considered. The static fluxes are assumed to follow the fundamental-mode distribution. The associated problem concerning how big the detectors must be when H is given, so that point kinetics become valid, has already been treated by Sheff and Albrecht (1966b).

For the calculation of the CPSD_R via equation (17) we need only the kinetic importance function ϕ_1^+ and the thermal-neutron flux ϕ_2. ϕ_1^+ can be represented as

$$\phi_1^+ = \phi_{1\mu}^+ + \phi_{1\lambda}^+, \tag{C.1}$$

$\phi_{1\mu}^+$, $\phi_{1\lambda}^+$ are the μ- and λ-terms, respectively, corresponding to the roots of equations (B.4a,b). Using the previous notation, these terms are given by

$$\phi_{1\mu}^+ = \frac{(\Sigma_2' + D_2\mu'^2)\Sigma_{1d} + \Sigma_R\Sigma_{2d}}{D_1D_2(\mu'^2+\lambda'^2)} g_\mu \tag{C.2a}$$

$$\phi_{1\lambda}^+ = -\frac{(\Sigma_2' - D_2\lambda'^2)\Sigma_{1d} + \Sigma_R\Sigma_{2d}}{D_1D_2(\mu'^2+\lambda'^2)} g_\lambda, \tag{C.2b}$$

where

$$g_\mu = \begin{cases} \dfrac{\sin \mu' x \sin \mu'(H-x_1)}{\mu' \sin \mu' H} & x \leqslant x_1 \\ \dfrac{\sin \mu'(H-x) \sin \mu' x_1}{\mu' \sin \mu' H} & x > x_1 \end{cases} \tag{C.3a}$$

$$g_\lambda = \begin{cases} \dfrac{\sinh \lambda' x \sinh \lambda'(H-x_1)}{\lambda' \sinh \lambda' H} & x \leqslant x_1 \\ \dfrac{\sinh \lambda'(H-x) \sinh \lambda' x_1}{\lambda' \sinh \lambda' H} & x > x_1. \end{cases} \tag{C.3b}$$

According to the decomposition of ϕ_1^+ into a μ-term and a λ-term, the CPSD_R consists of a sum of three components, a pure μ-component, a pure λ-component and a mixed $\mu\lambda$-component,

$$\mathrm{CPSD}_R = \mathrm{CPSD}_{R\mu} + \mathrm{CPSD}_{R\lambda} + \mathrm{CPSD}_{R\mu\lambda}. \tag{C.4}$$

For frequencies that are not too high, i.e. not much higher than a few times the critical break frequency α_c, the μ- and λ-roots of equations (B.4a,b) can approximately be represented (Behringer *et al.*, 1977) by

$$\mu'^2 \cong B^2(1-\mathscr{E}) \tag{C.5a}$$

$$\lambda'^2 \cong \frac{M^2}{\tau L^2} \tag{C.5b}$$

with

$$\mathscr{E} = \frac{kk_\infty}{B^2M^2G(\omega)}, \tag{C.5c}$$

B^2 is the static buckling ($=(\pi/H)^2$) and M^2 is the migration area ($=\tau+L^2$). G is the reactivity transfer function of equation (20a) with the neutron generation time Λ given by

$$\Lambda \cong \frac{1}{k}\left(\frac{1}{v_1\Sigma_1(1+\tau B^2)} + \frac{1}{v_2\Sigma_2(1+L^2B^2)}\right). \tag{C.5d}$$

The main approximations made for establishing the equations (C.5a,b) are neglect of the frequency dependence of Σ_1' and Σ_2' except in the small difference appearing in the square root of equation (B.4a). $\mathscr{E}$ is the governing parameter for the observation of possible space effects in the CPSD_R up to moderate frequencies. If $|\mathscr{E}|$ is $\ll 1$, the reactor will show point-kinetics behaviour. A critical reactor which fulfils this condition for a frequency up to the end of the plateau region in G, where G is approximately real, must have a size

$$H \ll \frac{\pi M}{\sqrt{\beta}}. \tag{C.6}$$

A reactor which satisfies the inequality (C.6) is defined as a small system. The usefulness of this definition is related to the frequency range which is normally involved in the reactor control. According to how well the condition (C.6) is fulfilled, the appearance of space effects will occur later or earlier with increasing frequency.

Let us further consider a small system with thermal-neutron detectors located not too close to the core boundaries, and restrict the frequency range up to moderate frequencies. Since $|\mu'^2|$ is $\ll|\lambda'^2|$, $\phi_{1\mu}^+$ and $\phi_{1\lambda}^+$ can be approximated by

$$\phi_{1\mu}^+ \cong \frac{2H\Sigma_R\Sigma_{2d}}{\pi^2D_1D_2\lambda'^2\mathscr{E}} \sin Bx \sin Bx_1 \tag{C.7a}$$

$$\phi_{1\lambda}^+ \cong -\frac{\Sigma_R\Sigma_{2d}}{2D_1D_2\lambda'^3} \exp(-\lambda'|x-x_1|) \tag{C.7b}$$

$\phi_{1\mu}^+$ of equation (C.7a) encompasses the whole reactor size, whereas $\phi_{1\lambda}^+$ of equation (C.7b) shows clearly a very local range. In order to obtain a rough estimate of how much the λ-term will contribute to the detector response relatively to the μ-term, let us assume a detector position in the core centre and a perturbation localized in a small region around the detector.

$$\delta S_1 = S_1(\omega)\delta(x-x_1);\ x_1 = \frac{H}{2}. \tag{C.8}$$

Substituting equations (C.7a,b) and (C.8) into equation (5) gives a ratio between the λ-component and the μ-component in the count-rate spectrum for a frequency point in the plateau region of G

$$\left|\frac{\delta R_\lambda}{\delta R_\mu}\right| \cong \frac{HL\beta(1-\rho^*)}{4M^2}, \tag{C.9}$$

where ρ^* is the \$-reactivity.

With the numerical data used in Section 6, and $H = 77.6$ cm, $\rho^* = -5$ \$, this ratio yields a value of 2.3%, indicating that the λ-term contributes very little in this frequency range. Due to the spatially very different ranges of the μ- and λ-terms, equation (C.9) represents an overestimate with regard to a source distributed throughout the core. Fig. C1 shows the negligible contribution of the λ-term to the CPSD_R, even at high frequencies. In these calculations no mathematical approximations were used. One sees a small contribution of the λ-term in the high-frequency range for detector locations rather near to the core boundaries and this contribution comes

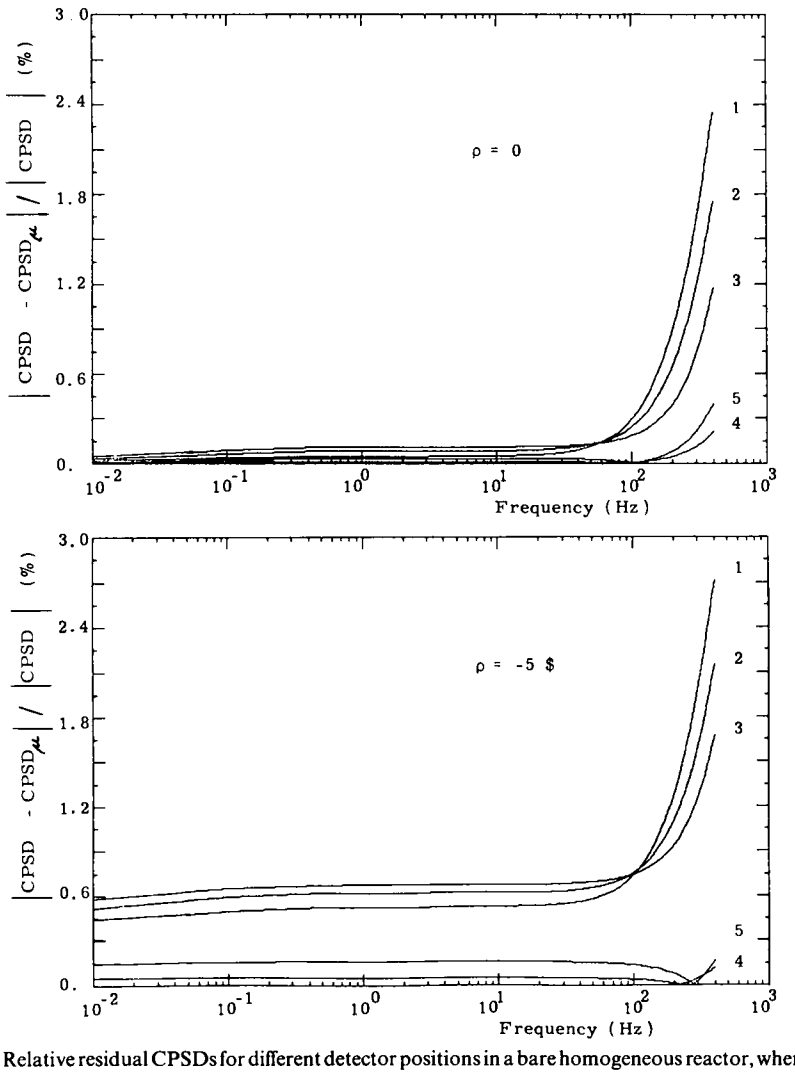

Fig. C1. Relative residual CPSDs for different detector positions in a bare homogeneous reactor, when the pure μ-term contribution is subtracted. $H = 77.6$ cm. Curve 1: detector position $\mathbf{x}_1 = \mathbf{x}_2 = 0.10 \times H$; curve 2: detector position $\mathbf{x}_1 = \mathbf{x}_2 = 0.25 \times H$; curve 3: detector position $\mathbf{x}_1 = \mathbf{x}_2 = 0.50 \times H$; curve 4: detector position $\mathbf{x}_1 = 0.10 \times H$, $\mathbf{x}_2 = 0.90 \times H$; curve 5: detector position $\mathbf{x}_1 = 0.25 \times H$, $\mathbf{x}_2 = 0.75 \times H$. The upper figure refers to the critical state, the lower figure to a subcritical state at -5 \$.

mainly from the mixed $\mu\lambda$-component in equation (C.4). The allowance for the neglect of the λ-term contribution makes the calculation of the CPSD_R by using the μ-term only, equivalent to an approach in one-group diffusion theory, except where the thermal diffusion length should be replaced by the migration length. The approximation of $\phi^+_{1\mu}$ by equation (C.7a) represents the first term of a more general representation of equation (C.2a) by an expansion in $\mathscr{E}$:

$$\phi^+_{1\mu} = (\cdots)\frac{1}{\mathscr{E}} + (\cdots) + (\cdots)\mathscr{E} + \cdots \qquad \text{(C.10)}$$

We will now show, that the use of only the first term in this expansion leads to the point kinetics result of the CPSD_R, which we will write in a form taken from the literature. It is to be noted that, if the second term in equation (C.10) is taken into account, this would correspond to the adiabatic approximation (Kosály *et al.*, 1977). If one writes for the thermal flux

$$\phi_2 = \phi_{2\max} \sin B\mathbf{x} \qquad \text{(C.11)}$$

and assumes that the thermal-neutron detectors might have different detection cross-sections $\Sigma_{2d1}, \Sigma_{2d2}$, equation (C.7a) can be brought into the form

$$\phi^+_{1\mu}(\mathbf{x}, \mathbf{x}_1, \omega) = 2\Sigma_{2d1}\phi_2(\mathbf{x}_1)\frac{G(\omega)}{Hv\Sigma_f\phi_{2\max}} \sin B\mathbf{x} \qquad \text{(C.12a)}$$

$$\phi^+_{1\mu}(\mathbf{x}, \mathbf{x}_2, \omega) = 2\Sigma_{2d2}\phi_2(\mathbf{x}_2)\frac{G(\omega)}{Hv\Sigma_f\phi_{2\max}} \sin B\mathbf{x} \qquad \text{(C.12b)}$$

Inserting equations (C.11) and (C.12a,b) into equation (17),

and neglecting the small delayed-neutron effect in h, gives

$$\mathrm{CPSD}_R(\mathbf{x}_1, \mathbf{x}_2, \omega)$$

$$= 2\frac{\overline{\nu(\nu-1)}}{\nu^2}\frac{4\Sigma_{2d1}\phi_2(\mathbf{x}_1)\Sigma_{2d2}\phi_2(\mathbf{x}_2)}{H^2\Sigma_f\phi_{2\max}}|G(\omega)|^2\int_0^H \mathrm{d}x\,\sin^3 Bx$$

$$= 2f\mathrm{D}\frac{R_1(\mathbf{x}_1)R_2(\mathbf{x}_2)}{F}|G(\omega)|^2 \qquad \text{(C.13)}$$

D is the Diven factor, defined by

$$\mathrm{D} = \frac{\overline{\nu(\nu-1)}}{\nu^2} \qquad \text{(C.14a)}$$

F is the fission-rate in the system (per unit area in the 1-D model), given by

$$F = \Sigma_f\int_0^H \mathrm{d}x\ \phi_2(x) \qquad \text{(C.14b)}$$

f is a spatial form factor of order unity introduced by Otsuka and Iijima (1965) to correct results derived from space-independent treatment for finite reactor geometry and spatial fission-rate distribution. It amounts, here, to

$$f = \frac{32}{3\pi^2} = 1.08 \qquad \text{(C.14c)}$$

and R_1, R_2 are the detector count-rates

$$R_1(\mathbf{x}_1) = \Sigma_{2d1}\phi_2(\mathbf{x}_1) \qquad \text{(C.14d)}$$

$$R_2(\mathbf{x}_2) = \Sigma_{2d2}\phi_2(\mathbf{x}_2). \qquad \text{(C.14e)}$$

If one regards the normalized CPSD_R, $\mathrm{NCPSD}_R = \mathrm{CPSD}_R/R_1R_2$ as a measure of space-dependence for any detector locations $\mathbf{x}_1, \mathbf{x}_2$ in the system, this quantity is clearly space-independent for the result of equation (C.13). Equation (C.13) can be altered to a slightly different form by introducing local-detector efficiencies:

$$w_1(\mathbf{x}_1) = R_1(\mathbf{x}_1)/F \qquad \text{(C.15a)}$$

$$w_2(\mathbf{x}_2) = R_2(\mathbf{x}_2)/F. \qquad \text{(C.15b)}$$

This allows one to write for equation (C.13):

$$\mathrm{CPSD}_R(\mathbf{x}_1, \mathbf{x}_2, \omega) = 2f\mathrm{D}w_1(\mathbf{x}_1)w_2(\mathbf{x}_2)F|G(\omega)|^2. \qquad \text{(C.16)}$$

The definition of the local detector efficiency corresponds to the experimental result of Thomas *et al.* (1973) who found the space dependence of detector efficiency to be proportional to that of average detector count-rates.

If one distributes the detectors uniformly through the reactor by integrating over $\mathbf{x}_1$ and $\mathbf{x}_2$, equation (C.16) reduces to the well-known point-reactor result (see e.g. Williams, 1974):

$$\mathrm{CPSD}_{RD}(\omega) = 2f\mathrm{D}W_1W_2F|G(\omega)|^2 \qquad \text{(C.17)}$$

where W_1, W_2 have the usual meaning of detector efficiency.

Let us briefly consider the other case of the infinite medium approach. If H is very large and both detectors are located far away from the core boundaries, $\phi^+_{1\mu}$ becomes

$$\phi^+_{1\mu}(\mathbf{x}, \mathbf{x}_1, \omega) \cong \frac{\Sigma_{2d1}}{2\nu\Sigma_f}G_\infty(\omega)\mathrm{T}(\omega)\exp[-\mathrm{T}(\omega)|\mathbf{x}-\mathbf{x}_1|] \qquad \text{(C.18a)}$$

$$\phi^+_{1\mu}(\mathbf{x}, \mathbf{x}_2, \omega) \cong \frac{\Sigma_{2d2}}{2\nu\Sigma_f}G_\infty(\omega)\mathrm{T}(\omega)\exp[-\mathrm{T}(\omega)|\mathbf{x}-\mathbf{x}_2|], \qquad \text{(C.18b)}$$

where $1/\mathrm{T}$ is a spatial relaxation length following from

$$\frac{1}{\mathrm{T}^2} = \frac{M^2}{k}G_\infty(\omega), \qquad \text{(C.19)}$$

here, G_∞ is the reactivity transfer function of the infinite reactor. The resulting CPSD_R can be written as

$$\mathrm{CPSD}_R \cong 2\mathrm{D}w_1w_2F|G_\infty|^2$$

$$\times\frac{H}{4}\left[\frac{\exp(-\mathrm{T}^*|\mathbf{x}_2-\mathbf{x}_1|)+\exp(-\mathrm{T}|\mathbf{x}_2-\mathbf{x}_1|)}{\frac{1}{\mathrm{T}^*}+\frac{1}{\mathrm{T}}}\right.$$

$$\left.+\frac{\exp(-\mathrm{T}^*|\mathbf{x}_2-\mathbf{x}_1|)-\exp(-\mathrm{T}|\mathbf{x}_2-\mathbf{x}_1|)}{\frac{1}{\mathrm{T}^*}-\frac{1}{\mathrm{T}}}\right]. \qquad \text{(C.20)}$$

The NCPSD_R of equation (C.20) is obviously strongly space dependent. A detector never sees the whole neutron field, but only a part determined by the spatial relaxation length. This part decreases with increasing frequency. There is a common spatial region, where the visual ranges of both detectors overlap. It is this common region of the neutron field which contributes to the CPSD_R. The further apart the detectors are spaced the smaller it is, and must finally vanish, when $|\mathbf{x}_2-\mathbf{x}_1|$ is very large.

Inspection of equation (C.20) shows, that the frequency dependence of the CPSD_R in a very large multiplying medium is different from the result of equation (C.16) for a small reactor. An expression can easily be obtained for the case of overlapping detector locations. It yields in the prompt-neutron kinetics approximation:

$$\mathrm{CPSD}_R(\mathbf{x}_2 = \mathbf{x}_1, \omega) \sim \frac{1}{\sqrt{(\omega^2+\alpha^2)}\cdot\sqrt{[\alpha+\sqrt{(\omega^2+\alpha^2)}]}}. \qquad \text{(C.21)}$$

The result of equation (C.21) is in agreement with the form derived for plate detectors by Natelson *et al.* (1966) and Williams (1966). By summing equation (C.20) for the case of distributed detectors, again the point-reactor CPSD_R must result. An infinite medium containing uniformly-distributed idealized detectors must be equivalent to a point reactor or space-independent reactor since the neutrons from all fission sources have an equal probability of being detected. The integration of equation (C.20) over $\mathbf{x}_1$ and $\mathbf{x}_2$ gives

$$\mathrm{CPSD}_{RD}(\omega) = 2\mathrm{D}W_1W_2F|G_\infty(\omega)|^2 \qquad \text{(C.22)}$$

Equation (C.22) must be regarded in units of volume. It is necessary after the integration of equation (C.20) to divide by H before taking the limit for $H \to \infty$, since one cannot have a *finite neutron flux and a finite number of neutrons in an infinite* reactor at the same time.

Finally, we should like to make an observation concerning the fast-thermal CPSD-technique for measuring the thermal-neutron lifetime. If one locates a fast-neutron detector and a thermal-neutron detector closely together in the critical reactor, i.e. ideally at the same space point, any phase relationships involved in the space integration are cancelled. The only terms which can give rise to a phase difference between the detector signals are the complex nominators in the first factors in equations (C.2a,b). Since for well-centred detector positions the λ-component contribution can be neglected, even at high frequencies, and the μ'^2-term or $\mathscr{E}$-term, respectively, in the nominator of the μ-component factor (equation (C.2a)) is a second-order effect, there remains a dominating phase satisfying the relationship $\mathrm{tg}\ \varphi = -\omega\Lambda_{\mathrm{th}}$ with A_{th} defined by $1/v_2\Sigma_2(1+L^2B^2)$. This relationship is a typical high-frequency effect. The phase-plot from an incore measurement performed by Penland *et al.* (1971) shows a linear relationship in the considered frequency range up to 800 Hz.